

Void growth within Li electrodes in solid electrolyte cells

J.A.B. Agier^a, S.S. Shishvan^{b,a}, N.A. Fleck^a and V.S. Deshpande^{a*}

^a *Department of Engineering, University of Cambridge, Cambridge CB2 1PZ, UK*

^b *Department of Structural Engineering, University of Tabriz, Tabriz, Iran*

Abstract

The growth of voids at the electrode/electrolyte interface of a solid state Li battery is analysed by establishing a framework that uses the Onsager formalism to couple the power-law creep deformation of the Li electrode and flux of Li⁺ through a single-ion conductor solid electrolyte. For realistic combinations of the interfacial resistance and electrolyte conductivity, standard Butler-Volmer kinetics for the interfacial flux does not provide sufficient flux focussing to initiate void growth and so a modified kinetics is adopted where the interfacial resistance is decreased by the presence of dislocations within the creeping Li electrode. Micron-sized pre-existing voids shrink under stripping conditions as flux focussing on the periphery of these voids is always low. However, spatially inhomogeneous creep in the electrode around a hemispherical impurity particle reduces the interfacial resistance with consequent significant flux focussing at the periphery of the impurity. This flux focussing results in void growth with two distinct regimes of behaviour: (i) at low currents stable but small voids form while (ii) at higher currents large voids form but these ultimately collapse. No conditions are identified for which isolated voids are predicted to grow larger than 10 μm in size suggesting that cell failure does not occur by the growth of isolated voids. We therefore propose a hypothesis for the coalescence of voids that initiate around impurity particles being deposited on the interface during stripping of the electrode. The ensuing predictions are consistent with measurements of cell failure and provide clues of the failure mechanisms due to void growth.

Keywords: Ceramic electrolyte, solid-state battery, void-growth, Butler-Volmer kinetics

* Corresponding author. E-mail address: vsd20@cam.ac.uk

1. Introduction

Batteries with reactive metal anodes, such as Li or Na, have the potential to deliver higher specific energies [1, 2]. However, liquid electrolyte batteries with a Li metal electrode experience dendrite nucleation and growth from the Li electrode/electrolyte interface. These features can take the form of mossy growth [3], needle-protrusions or globular extrusions [4, 5] and can grow across the electrolyte to short-circuit the battery. It was hoped that solid-state cells composed of stiff ceramic electrolytes would not experience dendrite nucleation and growth and would also deliver enhanced safety along with higher specific energies [6, 7]. In reality, solid-state cells also fail by short-circuiting due to the penetration of Li filaments through the ceramic electrolyte. This failure mode operates at currents exceeding the so-called “critical current density” [8, 9]; below the critical current density the battery can cycle stably.

Bruce and co-workers [10, 11] have recently observed two distinct critical current densities: the critical current for stripping (CCS), and the critical current for plating (CCP). They observed that Li filaments initiate and grow in Argyrodite ($\text{Li}_6\text{PS}_5\text{Cl}$) electrolytes when Li metal is plated onto the electrode at a current that exceeds the CCP [10, 11]. Conversely, stripping Li metal electrode leads to the formation of voids in the electrode when the CCS is exceeded, resulting in a concentration of current at the remaining areas of contact between the electrode and electrolyte. Typically, the value of CCS is less than that of CCP and experiments suggest that Li filaments preferentially grow in the vicinity of voids at the electrode/electrolyte interfaces with voids reducing the CCP. Similar observations of two distinct critical current densities corresponding to plating and stripping have been reported in a wide range of solid-state electrolytes with reactive metal electrodes including Li/LLZO (Li stuffed garnet $\text{Li}_7\text{La}_3\text{Zr}_2\text{O}_{12}$) [12, 13] and Na/Na- β'' -alumina [14] interfaces. Thus, the prevention of void

growth is technologically important and a number of attempts have been made to design an architected electrode [15-17] to exploit creep for stabilising the electrode/electrolyte interface.

A fundamental understanding of the mechanism of void formation and growth at the electrode/electrolyte interface is needed to improve battery performance. Recently, a series of elementary models [12, 18, 19] have been proposed suggesting that flux focusing around the periphery of an initial imperfection on the electrode/electrolyte interface is the cause of void growth. The basic hypothesis is sketched in Fig. 1a and is explained as follows. Imperfections along the interface and/or loss of contact between the electrolyte and the electrode due to surface roughness give rise to a circular disk of diameter $2a_0$ where flux of the Li^+ ions is blocked. The resulting spatially inhomogeneous electric field concentrates the Li flux around the periphery of the imperfection, which in turn induces creep deformation of the electrode and growth of the void. However, this simple explanation, based on Butler-Volmer kinetics, has a flaw as elucidated by Roy et al. [19] and enunciated as follows.

Define the concentration factor K_j for flux focussing as the ratio of the maximum interfacial flux at the periphery of the imperfection, i.e., $\max(j)$, to the far-field interfacial flux j_∞ . Predictions using the usual Butler-Volmer kinetics by Roy et al. [19] of K_j as a function of $\bar{a}_0 \equiv a_0/(\kappa Z_0)$ are plotted in Fig. 1b; here, κ is the ionic conductivity of the electrolyte and Z_0 is the interfacial resistance. We emphasise that the product κZ_0 defines a material length scale and using typical values for Li/LLZO/Li cells, viz. $\kappa = 0.4 \text{ mS cm}^{-1}$ and $Z_0 = 5 \text{ } \Omega\text{cm}^2$ [20], we obtain $\kappa Z_0 \approx 20 \text{ } \mu\text{m}$. Thus, given that the flux concentration $K_j < 3$ for $\bar{a}_0 < 10$ (Fig. 1b), this suggests that flux focussing remains small for imperfections of size $< 200 \text{ } \mu\text{m}$. In fact, Roy et al. [19] demonstrated that, for $\kappa Z_0 = 20 \text{ } \mu\text{m}$, no void growth will occur from imperfections $< 1 \text{ mm}$ in size. Interfacial imperfections $> 1 \text{ mm}$ are unrealistic and in fact

while voids do grow to $> 100 \mu\text{m}$ in size [10], they are typically less than a few microns in diameter in the early stages of growth.

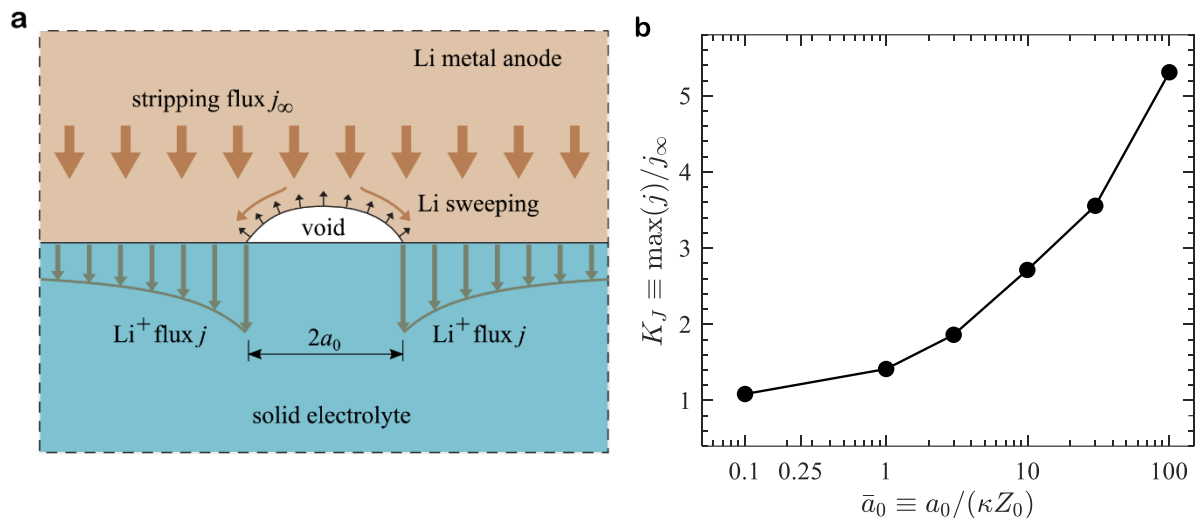


Figure 1: (a) Sketch showing flux focussing over the periphery of the imperfection which sweeps Li over the void/imperfection surface and tends to grow a void at the interface, while the overall stripping flux in the electrode tends to close the void. (b) Predictions [19] using standard Butler-Volmer kinetics of the flux concentration factor K_J around the periphery of the imperfection as a function of the normalised imperfection size $\bar{a}_0 \equiv a_0/(\kappa Z_0)$.

Butler-Volmer kinetics, as employed in most of the literature including the work of Roy et al. [19], adequately describes the flux across the Li electrode/electrolyte interface when the electrode is not deforming. However, if the Li electrode maintains contact with a rigid solid electrolyte, a non-deforming electrode implies spatially uniform stripping/plating over the interface. But void growth implies spatially non-uniform stripping and is usually accompanied by power-law creep deformation of the electrode. The mechanism of power-law creep is climb-mediated glide of dislocations [21] and Shishvan et al. [22] argued that nucleation and multiplication of dislocations strongly influence the interface kinetics. Accounting for the influence of dislocations, Shishvan et al. [22] showed that void growth can initiate from sub-

micron scale impurity particles on the electrode/electrolyte interfaces due to a reduction in the interfacial resistance around the periphery of the impurity particles. The initiation of these voids is suppressed by the imposition of a stack pressure and the predictions of Shishvan et al. [22] are consistent with measurements reported by Wang et al. [13]. While Shishvan et al. [22] modelled the initiation of void growth from sub-micron sized impurity particles, it is known from experiments that voids can grow to sizes in excess of 100 μm [10]. The mechanism by which voids can grow to such large sizes remains unclear. The focus of this study is to extend the void initiation formulation of Shishvan et al. [22] to model the growth of voids at the electrode/electrolyte interface and propose a hypothesis for cell failure based on void coalescence.

2. Problem definition and model formulation

We consider the axi-symmetric problem sketched in Fig. 2a where Li^+ is progressively stripped from the electrode across the Li electrode/LLZO electrolyte interface. Envision that a small hemispherical impurity particle, or hemispherical void, of radius a_0 exists on the interface, thereby preventing flux across the interface over a circular patch of radius a_0 . The Li electrode maintains contact with the rigid solid electrolyte, and the growth of void is accompanied by deformation of the Li electrode via climb-mediated glide of dislocations, i.e., power-law creep [21]. We shall first summarise some key aspects of the thermodynamics of a Li electrode containing dislocations and vacancies as developed in [22]. Subsequently, we use the Onsager [23-24] formalism for non-equilibrium processes to develop an interfacial flux law for the case when a growing void exists within the electrode.

2.1 Summary of the effect of dislocations on interface kinetics

Standard Butler-Volmer kinetics neglects the effect of dislocations in the Li electrode as the dislocation density in Li is vanishingly small in the absence of creep deformation. In creep deformation, the dislocation density increases with increasing deviatoric stress [21, 25] and Shishvan et al. [22] argued that the presence of the dislocations changes both the availability of lattice sites and the enthalpy of the Li^+ ions in the electrode. Consequently, creep of Li affects interface kinetics with the two important effects of dislocations being:

- (i) The presence of dislocations results in a small expansion of the metal which in turn increases the effective fraction of vacant lattice sites within the Li electrode. This effective fraction $\hat{\theta}_v$ of vacant sites at a temperature T is related to the density ρ_d of dislocations of Burgers vector b via

$$\hat{\theta}_v = \exp\left(-\frac{h_v}{RT}\right) + \alpha \frac{\Omega_{\text{Li}}(\rho_d b^2)}{\Omega_v}, \quad (1)$$

where h_v is the enthalpy of vacancy formation in Li with R the gas constant, Ω_v and Ω_{Li} are the molar volume of vacancies and Li, respectively, while the constant α depends on the metal crystal structure. For example, $\alpha \approx 0.25$ for fcc Cu and ≈ 2.7 for bcc Fe [26]. The expression (1) is a sum of the fraction of vacancies in the Li (first term) and a term proportional to α that models the extra space due to expansion of the lattice by dislocations.

- (ii) The distortion of the Li lattice both within the dislocation cores and by the long-range elastic fields of the dislocations enhances the enthalpy of the Li^+ ions.

Using (1) and the assumption that the fraction of effective vacant sites $\hat{\theta}_v$ is such that it minimizes the free-energy for a given ρ_d (i.e., an equilibrium assumption), Shishvan et al. [22] calculated the enthalpy and entropy of the electrode as a function of the dislocation density.

They showed that the standard chemical potential of the Li^+ ions (i.e., chemical potentials absent the configurational entropy contribution) within the electrode at an electric potential ϕ_p and subjected to a pressure p is given by $\chi_{\text{Li}^+} = \mu_0 + RT \ln(\hat{\theta}_v) + F\phi_p + p\Omega_{\text{Li}}$ where F is the Faraday constant and μ_0 the reference chemical potential at zero pressure and electric potential. Combining this relation with (1), we observe that χ_{Li^+} increases due to the presence of dislocations because of the enhancement in the enthalpy due to distortion of the Li lattice associated with dislocations. Given this expression for χ_{Li^+} , Shishvan et al. [22] evaluated the interfacial barrier for Li^+ ions to cross the electrode/electrolyte interface using the usual Butler-Volmer assumption that the barrier is set by the weighted mean of the standard chemical potentials of the two end-states. The increase in χ_{Li^+} reduces the barrier for the crossing of Li^+ ions from the electrode to the electrolyte and thereby reduces the interfacial resistance Z . Specifically, Z is related to the resistance Z_0 in the absence of dislocations by

$$Z = Z_0 \hat{\theta}_v^{\beta-1} \exp\left[-\frac{(1-\beta)h_v}{RT}\right], \quad (2)$$

where $0 \leq \beta \leq 1$ is the Butler-Volmer symmetry factor. Typically, β equals 0.5 and, upon combining (1) and (2), we observe that the interfacial resistance Z decreases with increasing dislocation density ρ_d .

Following [25], the dislocation density in the Li metal subjected to a stress σ scales as $\rho_d \propto (1/b^2)(\sigma/G_{\text{Li}})$, where G_{Li} is the shear modulus of Li. Consequently, the flux across the interface is strongly coupled to the creep deformation of the electrode. An increase in creep strain rate (or equivalently an increase in stress) reduces the interfacial resistance in the vicinity of the imperfection and thereby increases the flux concentration. This flux concentration in turn influences the creep of the electrode, resulting in strong two-way coupling between creep deformation and interface kinetics.

2.2 Interfacial flux for a Li electrode with a growing void

A flux that varies along the electrode/electrolyte interface (which will occur during void growth within the electrode) necessarily requires deformation of the electrode. We calculate the interfacial flux by developing a variational principle [23-24] wherein the rate of loss of potential energy $\dot{\Pi}$ of the electrode drives not only the dissipation due to creep within the electrode but also the dissipation associated with the interfacial flux.

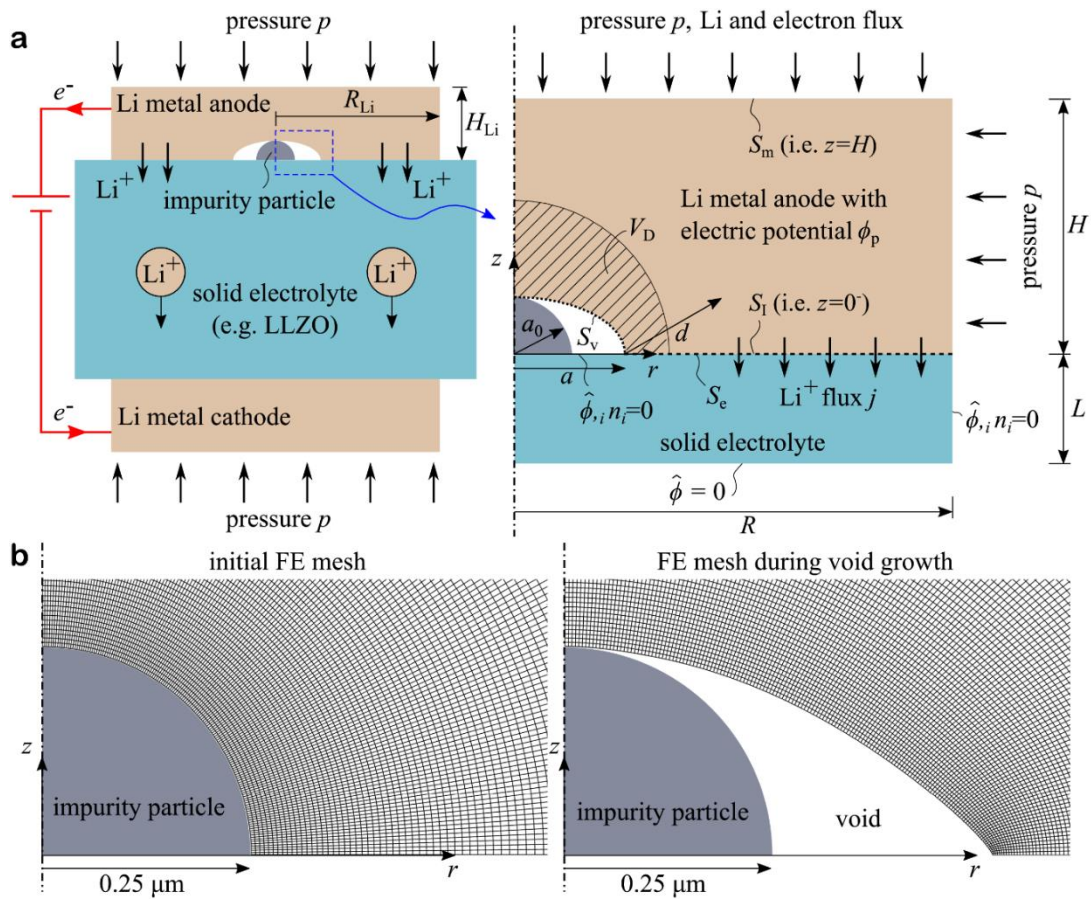


Figure 2: (a) Sketch of the axi-symmetric problem with an isolated hemispherical impurity particle on the interface of the stripping electrode/solid electrolyte. The symmetric cell shown is powered by an external power source with the cell subjected to a stack pressure p . The inset shows the small region of the cell that is analysed here with key features labelled. The (r, z) co-ordinate system is included in the inset. (b) A representative example of the evolution of the “moving mesh” in the electrode around the impurity.

A large electrode (as shown in Fig. 2a with radius R_{Li} and thickness H_{Li}), in contact with an electrolyte, is maintained at an electric potential ϕ_p and is subjected to a stack pressure p . The primarily electrode deforms over a local volume V_D , at the location where void growth may occur near the electrode/electrolyte interface (see inset of Fig. 2a). We analyse a small spatially fixed portion of the Li cell as shown by the dashed lines in Fig. 2a. Within this region analysed is a volume V of the electrode that is sufficiently large that the remote boundaries are far from V_D : the remote Li electrode boundaries are non-deforming. The surface of V is denoted by S , with S_m ($z = H$ in Fig. 2a) and S_l ($z = 0^-$ in Fig. 2a) denoting the top and bottom surfaces, respectively. The Li in V occupies a region $V_{\text{Li}} \leq V$ as the impurity and/or void are also part of V . It is instructive to separate the bottom surface S_b of V_{Li} into two portions such that $S_b \equiv S_e \cup S_v$. Here, S_e is just within the electrolyte along the portion of the interface where the Li is in contact with the electrolyte (i.e., S_e is common to S_b and S_l) and S_v is the void surface or impurity particle surface (if the Li is detached from the impurity, S_v is the traction-free void surface while it is the impurity particle surface if the Li is in contact with the impurity). Importantly, as the void grows S_e and S_v are not spatially fixed boundaries. By contrast, the lateral and top boundaries of V_{Li} are spatially fixed. Thus, while the region V is a spatially fixed region, the region V_{Li} is a mixed Eulerian/Lagrangian domain. In developing a variational principle, it is convenient to define V as the system and consider the rate of potential energy change and dissipation within this system.

The Li fluxes across the lateral boundaries of V vanish while the Li flux and stack pressure p on the top surface S_m of V is spatially uniform and normal to the surface. The chemical potential of the Li entering V via top surface S_m is $\mu_{\text{Li}} = \mu_0 + p\Omega_{\text{Li}}$, where μ_0 is the reference chemical potential of Li. Along the S_e portion of bottom surface of V , the chemical potential of Li^+

exiting the system is $\mu_{\text{Li}^+}^e = \mu_0^e + F\phi$, where μ_0^e is the reference chemical potential of Li in the electrolyte and ϕ is the electric potential in the electrolyte at the interface. Write the chemical potential of the electrons as $\mu_{\text{e}^-} = -F\phi_p$ while, under isothermal conditions for a region of fixed volume V , the rate of change of the Helmholtz free-energy of V is $\dot{A} = \dot{N}_{\text{Li}}\mu_0$ with \dot{N}_{Li} being the rate of change of Li content N_{Li} in V . The second law of thermodynamics requires that for an isothermal process the rate of change of potential energy $\dot{\Pi}$ of volume V satisfies the inequality

$$\dot{\Pi} \equiv \dot{A} + \frac{1}{F} \int_{S_m} \mu_{\text{Li}} j_i^{\text{Li}} n_i dS + \frac{1}{F} \int_{S_m} \mu_{\text{e}^-} j_i^{\text{e}^-} n_i dS + \frac{1}{F} \int_{S_e} \mu_{\text{Li}^+}^e j_i^{\text{Li}^+} n_i dS \leq 0, \quad (3)$$

where j_i^{Li} and $j_i^{\text{e}^-}$ are the fluxes of Li and electrons, respectively, across S_m while $j_i^{\text{Li}^+}$ is the Li^+ flux across S_e (the only flux leaving V over S_l is along S_e) with n_i denoting the normal to the respective surfaces. Note that in writing (3) we have neglected contributions from the work of adhesion between the Li and electrolyte and surface energy of Li. This assumption is justified by noting that the electrical energy and creep dissipation are significantly larger than the surface energy contributions and therefore this approximation is expected to result in negligible errors.

Conservation of charge (i.e., the volume V remains charge neutral) implies

$$-\int_{S_m} j_i^{\text{e}^-} n_i dS + \int_{S_e} j_i^{\text{Li}^+} n_i dS = 0, \quad (4)$$

while conservation of Li demands

$$\int_{S_m} j_i^{\text{Li}} n_i dS + \int_{S_e} j_i^{\text{Li}^+} n_i dS = -F\dot{N}_{\text{Li}}. \quad (5)$$

Upon substituting for the chemical potentials, viz. $\mu_{\text{Li}^+}^e = \mu_0^e + F\phi$, $\mu_{\text{e}^-} = -F\phi_p$ and $\mu_{\text{Li}} = \mu_0 + p\Omega_{\text{Li}}$, as well as recalling that p is spatially uniform over S_m it follows from (5) that

$$\dot{\Pi} = \frac{1}{F} \int_{S_e} (\mu_0^e - \mu_0 + F\phi) j_i^{\text{Li}^+} n_i dS - \phi_p \int_{S_m} j_i^{\text{el}^-} n_i dS + \frac{p\Omega_{\text{Li}}}{F} \int_{S_m} j_i^{\text{Li}} n_i dS. \quad (6)$$

The overpotential across the electrode/electrolyte interface is defined as $\eta \equiv \phi_p - (\phi + \mathcal{U})$

with the open circuit potential $\mathcal{U} \equiv (\mu_0^e - \mu_0)/F$. Now making use of (4) we obtain

$$\dot{\Pi} = - \int_{S_e} \eta j_i^{\text{Li}^+} n_i dS + \frac{p\Omega_{\text{Li}}}{F} \int_{S_m} j_i^{\text{Li}} n_i dS. \quad (7)$$

The decrease in potential energy of V is associated with dissipation in V by two mechanisms:

(i) dissipation related to the creep deformation of the bulk electrode and (ii) dissipation

associated with the flux of Li^+ across the electrode/electrolyte interface. First consider

dissipation in the bulk of the electrode due to incompressible creep flow of the Li. The

deviatoric stress $s_{ij} (\equiv \sigma_{ij} - (\sigma_{kk}/3)\delta_{ij})$ where σ_{ij} is the stress and δ_{ij} the Kronecker delta) in

the Li is obtained from a dissipation potential Φ_m via

$$s_{ij} \equiv \frac{\partial \Phi_m}{\partial \dot{\epsilon}_{ij}}, \quad (8)$$

where $\dot{\epsilon}_{ij}$ is an incompressible strain rate (i.e., $\dot{\epsilon}_{kk} = 0$). Note that $\Phi_m = 0$ in the void and/or

impurity particle. The dissipation rate per unit volume in the bulk electrode is $\dot{d}_m =$

$(\partial \Phi_m / \partial \dot{\epsilon}_{ij}) \dot{\epsilon}_{ij}$. Next consider the dissipation associated with flux across the

electrode/electrolyte interface. Following Shishvan et al. [22], we define an interface

dissipation potential $\Phi_I \equiv j^2 Z/2$ (with $j = j_i^{\text{Li}^+} n_i$) such that the dissipation rate per unit area

of interface is $\dot{d}_I = j(\partial \Phi_I / \partial j)$.

We can now proceed to derive the flux relation for the deforming electrode. Following [22],

define a functional

$$\Psi(\dot{\epsilon}_{ij}, j_i) \equiv \dot{\Pi} + \int_{S_e} \Phi_I dS + \int_V \Phi_m dV. \quad (9)$$

The variation $\delta\Psi$ with respect to arbitrary variations δj_i in flux is given by

$$\begin{aligned}
\delta\Psi &= -\frac{1}{F} \int_{S_e} \eta \delta j_i^{\text{Li}^+} n_i dS + \frac{p\Omega_{\text{Li}}}{F} \int_{S_m} \delta j_i^{\text{Li}} n_i dS + \int_{S_e} \frac{\partial\Phi_1}{\partial j} \delta j_i^{\text{Li}^+} n_i dS + \int_{V_{\text{Li}}} \frac{\partial\Phi_m}{\partial \dot{\epsilon}_{ij}} \delta \dot{\epsilon}_{ij} dV \\
&= \delta\dot{\Pi} + \int_{S_e} \delta \dot{d}_1 dS + \int_{V_{\text{Li}}} \delta \dot{d}_m dV,
\end{aligned} \tag{10}$$

where $\delta \dot{d}_m = s_{ij} \delta \dot{\epsilon}_{ij} = \sigma_{ij} \delta \dot{\epsilon}_{ij}$ since $\dot{\epsilon}_{kk} = 0$ and we have replaced the integral over V by the integral over V_{Li} since $\Phi_m = 0$ in the void and/or impurity particle. At equilibrium, arbitrary variations in the potential energy are balanced by the equivalent variations in the dissipation thereby requiring $\delta\Psi = 0$. Write v_i as the material velocity of the Li in the electrode and write the traction on the surface S_{Li} of the volume V_{Li} as $T_i \equiv \sigma_{ij} n_j$, where n_i is the outward normal to S_{Li} . Then, application of the divergence theorem, along with the stress equilibrium relation $\sigma_{ij,j} = 0$ and the compatibility relation $\dot{\epsilon}_{ij} = 0.5(v_{i,j} + v_{j,i})$ gives

$$\int_{S_{\text{Li}}} T_i \delta v_i dS + \int_{S_e} Z j \delta j dS = \int_{S_e} \eta \delta j_i^{\text{Li}^+} n_i dS - \frac{p\Omega_{\text{Li}}}{F} \int_{S_m} \delta j_i^{\text{Li}} n_i dS. \tag{11}$$

On S_v , the traction T_i vanishes where the Li has detached from the impurity, and $v_i n_i = 0$ where the Li remains in contact with the impurity particle. Now write t_i as a unit vector along the interfaces S_v and S_e , and assume that the Li is free to slip over both the impurity particle and the electrolyte surface S_e such that $T_i t_i = 0$ on $S_v \cup S_e$. Then recalling that the flux vanishes on the lateral boundaries, (11) simplifies to

$$\int_{S_m} T_i \delta v_i dS + \int_{S_e} T_i \delta v_i dS + \int_{S_e} Z j \delta j dS = \int_{S_e} \eta \delta j_i^{\text{Li}^+} n_i dS - \frac{p\Omega_{\text{Li}}}{F} \int_{S_m} \delta j_i^{\text{Li}} n_i dS. \tag{12}$$

Upon recalling that $T_i = -p n_i$ and $v_i = j_i^{\text{Li}} \Omega_{\text{Li}} / F$ over S_m , and $v_i = j_i^{\text{Li}^+} \Omega_{\text{Li}} / F$ over S_e , it follows that

$$j = \frac{\eta - T_i n_i \Omega_{\text{Li}} / F}{Z}. \tag{13}$$

This is the usual form of the Butler-Volmer relation but here we have shown, using the Onsager [23-24] formalism, that it applies for a deforming electrode within which a void might grow.

Note that there are two sources for electro-mechanical coupling in (13): (i) the $T_i n_i \Omega_{Li}/F$ term in the numerator which is traditionally thought to be the source of the coupling and (ii) the interfacial resistance Z given by (2) that depends upon the dislocation density and hence also, in turn, on the mechanical state of the electrode. Typically, $|T_i n_i \Omega_{Li}/(F\eta)| \ll 1$ and thus, as discussed in Roy et al. [19] and shown explicitly by Shishvan et al. [22], this term has little influence on the solution. We shall proceed to show that the strong electro-mechanical coupling which gives rise to void growth is an outcome of the changes in the interfacial resistance Z due to dislocations associated with the creep deformation of the electrode.

2.3 *The governing equations and constitutive models*

The governing equations for the mechanical fields within the electrode are strongly coupled to the electrochemical fields within the electrolyte and vice-versa. Here, we summarize these coupled governing equations and the associated constitutive models.

2.3.1 *Li electrode*

There is general agreement in the literature that Li, at room temperature, behaves as an incompressible creeping solid [21, 27]. Thus, the Li electrode is required to satisfy static stress equilibrium $\sigma_{ij,j} = 0$ while the velocity field is divergence-free, i.e., $v_{i,i} = 0$. The strain rate $\dot{\epsilon}_{ij} \equiv 0.5(v_{i,j} + v_{j,i})$ and the deviatoric stress are related via (8) with incompressibility implying that the hydrostatic stress σ_{kk} is solved as a Lagrange multiplier to ensure $\dot{\epsilon}_{kk} = 0$. These governing equations together are referred to as the nonlinear Stokes equations which implies that the Li electrode is essentially treated as an incompressible fluid. At high levels of stress, dislocation creep is the dominant mechanism and the stress is related to strain rate via a power-law relation. At lower levels of stress, diffusional flow (i.e., either Coble creep or Nabarro-Herring creep depending on the grain size) dominates with the stress scaling linearly

with strain rate. We define a dissipation potential Φ_m in terms of a reference stress σ_0 and strain rate $\dot{\epsilon}_0$ as

$$\Phi_m \equiv \begin{cases} \frac{\sigma_0 \dot{\epsilon}_0}{n+1} \left(\frac{\dot{\epsilon}}{\dot{\epsilon}_0}\right)^{n+1} & \text{for } \dot{\epsilon} \geq \dot{\epsilon}_c \\ \frac{\sigma_0 \dot{\epsilon}_c}{2} \left(\frac{\dot{\epsilon}_c}{\dot{\epsilon}_0}\right)^n \left(\frac{\dot{\epsilon}}{\dot{\epsilon}_c}\right)^2 & \text{otherwise,} \end{cases} \quad (14)$$

where n is the power-law exponent. Here, $\dot{\epsilon} \equiv \sqrt{(2/3)\dot{\epsilon}_{ij}\dot{\epsilon}_{ij}}$ is the von-Mises effective strain rate in terms of the incompressible strain rate $\dot{\epsilon}_{ij}$ (i.e., $\dot{\epsilon}_{kk} = 0$) and $\dot{\epsilon}_c$ is the critical value of $\dot{\epsilon}$ at which creep response transitions from diffusional flow to power-law creep. For this incompressible material, the incompressible strain rate $\dot{\epsilon}_{ij}$ is related to the deviatoric stress s_{ij} via (8). The hydrostatic stress σ_{kk} is not specified by the constitutive relation and is treated as a Lagrange multiplier that enforces incompressibility. We emphasize that (14) along with the associated parameters is an empirical relation based on creep measurements [21, 27] for polycrystalline Li and thus implicitly includes the effect of grain boundaries on the creep of polycrystalline Li. Typical grain sizes of Li electrodes are $\sim 150 \mu\text{m}$ [27]. We shall show that the length-scale for void growth is $\ll \sim 150 \mu\text{m}$ and thus neglecting the effects of grain boundary heterogeneities on void growth is a reasonable assumption.

It remains to relate the dislocation density ρ_d to the deformation of the Li. In the linear viscous regime, deformation is an outcome of vacancy diffusion and the dislocation density is negligible. In contrast, power-law creep is a consequence of climb-assisted dislocation glide and there exists a large literature on the dependence of dislocation density upon magnitude of stress for a range of metals [28]. However, to-date there have been no such measurements reported for Li and hence we shall follow [22] in utilising the model of Weertman [25] which was motivated by measurements on metals such as aluminium. We specify that the dislocation

density scales with the von-Mises effective stress $\sigma \equiv \sqrt{(3/2)s_{ij}s_{ij}}$ and the shear modulus G_{Li} of Li as

$$\rho_d = \begin{cases} k \left(\frac{\sigma - \sigma_c}{G_{\text{Li}}b} \right)^2 & \text{for } \sigma \geq \sigma_c \\ 0 & \text{otherwise,} \end{cases} \quad (15)$$

where k is a non-dimensional constant on the order of unity. In (15), $\sigma_c \equiv \sigma_0(\dot{\epsilon}_c/\dot{\epsilon}_0)^n$ is the value of σ at which the creep behaviour transitions from linear viscous to power-law so that the above relation assumes that the dislocation density vanishes in the linear viscous regime.

2.3.2 Solid electrolyte

Now, consider the ceramic single-ion conductor electrolyte. We make two simplifying assumptions that have been widely used for such systems to reduce the complexity of the governing equations and allow for all of the required material and interfacial properties for Li/LLZO/Li symmetric cells to be directly obtained from measurements already reported in the literature. These assumptions are: (i) the electrolyte is electroneutral [29, 30] so that the concentration of Li^+ within a homogeneous electrolyte is spatially uniform and balanced by the immobile anions and (ii) the molar volume Ω_e of Li within the electrolyte is assumed to be zero [31-33]. Assumption (ii) is justified by speculating that the Li in Li-stuffed garnet-type ceramic electrolytes lies within a rigid ceramic skeleton which does not deform upon removal/addition of a Li atom. These assumptions significantly reduce the complexity of the governing equations which we now proceed to describe.

The electrolyte is treated as an isotropic linear dielectric. Gauss's law for a linear dielectric of permittivity \mathcal{E} requires that the electric field E_i satisfies $\mathcal{E}E_{i,i} = \rho_f$ where ρ_f is the density of free-charge. Further, in electrostatics, the Maxwell-Faraday equation is automatically satisfied

by defining $E_i \equiv -\phi_{,i}$, where ϕ is the electric potential and so Gauss's law reduces to $\mathcal{E}\phi_{,ii} = -\rho_f$. However, since we have restricted our analysis to the case of an electroneutral electrolyte where the concentration of the Li^+ remains fixed at c_e^0 , the density of free-charge ρ_f vanishes and Gauss's law for the electrolyte reduces to $\phi_{,ii} = 0$. The flux of Li^+ in the electrolyte is specified in terms of the local driving force given by the gradient of chemical potential of Li^+ . Specifically, this driving force is $f_i \equiv -\partial\mu_{\text{Li}^+}^e/\partial x_i$ and the flux in the electroneutral electrolyte is $h_i \equiv mc_e^0 f_i$, where m is the mobility of Li^+ in the electrolyte. Typically, the flux in the electrolyte is measured in terms of the ionic current $j_i = Fh_i$ of the Li^+ ions, with the mobility written in terms of an ionic conductivity defined as $\kappa \equiv j_1/E_1$ for an electrical field applied in the 1-direction. Thus, upon setting $\kappa = mc_e^0 F$ the current is related to the gradient of the electric potential as $j_i = -\kappa\phi_{,i}$ which is essentially a statement of Ohm's law. The divergence of the current is proportional to the rate of change of the concentration of Li^+ ions and since we are constraining the electrolyte to remain electroneutral the current is divergence-free. The flux balance law then reduces to $\phi_{,ii} = 0$. Thus, for the electroneutral electrolyte with $\Omega_e = 0$, the electrical and Li^+ flux balance laws reduce to a single governing equation given by the Laplace equation $\phi_{,ii} = 0$ that needs to be solved with appropriate boundary conditions. We emphasize that this reduction in the number of independent governing equations implies that no solutions exist for certain problems (e.g., electrolyte loaded by blocking electrodes that impose an electrical potential across the electrolyte but prohibit the flux of Li^+ across the electrolyte/electrode interfaces). However, the electroneutrality assumption admits solutions for the boundary value problems analysed here and hence this simplification is considered appropriate for this study. In the following, it is convenient to define an electric potential $\hat{\phi} \equiv \phi + \mathcal{U}$ with the governing equation in the electrolyte being $\hat{\phi}_{,ii} = 0$: this allows us to specify all boundary conditions for the electrolyte in terms of $\hat{\phi}$ without the need to explicitly specify \mathcal{U} .

2.4 Boundary conditions

We consider the case of an isolated hemispherical impurity/void of radius a_0 on the electrode/electrolyte interface as shown in Fig. 2a and analyse a cylindrical region of radius R with the electrode/electrolyte interface located at $z = 0$ and the bottom surface of the electrolyte at $z = -L$ while the top surface of the electrode is at $z = H$ (see inset of Fig. 2a). With $L \gg a_0$, this rear surface of the electrolyte is far from the imperfection and the electric field at $z = -L$ is one-dimensional. Thus, without loss of generality we can set $\hat{\phi} = 0$ on $z = -L$. Similarly, the cylindrical surface at $r = R$ is also far from the imperfection and there is no flux in the electrolyte across this surface. The boundary conditions (in cylindrical co-ordinates) for the Laplace equation $\hat{\phi}_{,ii} = 0$ governing the electric potential within the electrolyte are:

$$\begin{aligned} \hat{\phi} &= 0 & \text{over } z &= -L, \\ \hat{\phi}_{,i}n_i &= 0 & \text{over } r &= R, \\ \hat{\phi}_{,i}n_i &= 0 & \text{over the portion of } z &= 0 \text{ that is not part of } S_e, \\ \hat{\phi}_{,i}n_i &= -j/\kappa & \text{over } S_e. \end{aligned} \tag{16}$$

Here, n_i is the outward normal to the appropriate surfaces of the electrolyte and the current j is given by rewriting Eq. (13) as

$$j = \frac{(\phi_p - \hat{\phi}) - T_i n_i \Omega_{Li}/F}{Z}, \tag{17}$$

where ϕ_p is the imposed value of the electrode potential and T_i the traction on the electrolyte surface in contact with the electrode (which is equal and opposite to the traction on the electrode surface). Both the traction T_i on the electrolyte surface and the interfacial resistance Z are not known without a solution of the creep deformation within the electrode, i.e., electrical fields within the electrolyte are fully coupled with the mechanical deformation of the electrode.

We analyse the central region V_{Li} which is bounded by a mixture of Eulerian and Lagrangian surfaces. The Eulerian surfaces (i.e., surfaces fixed in space with material flowing across them)

are the top surface located at $z = H$ (i.e., S_m) and the side surface at $r = R$. The boundary conditions along the bottom surface $S_b \equiv S_e \cup S_v$ are more complex and evolve with the growth of the void. The surface S_b has two portions: (i) a surface S_e along $z = 0$ that is in contact with the electrolyte and located at $r > a$, where $a \geq a_0$ is the current radius of the void along $z = 0$ (inset of Fig. 2a) and (ii) the void surface S_v located at $r < a$ and $z > 0$ (inset of Fig. 2a). The surface S_e is an Eulerian surface that is always at $z = 0$ with Li^+ flowing across it from the electrode to the electrolyte while S_v is a Lagrangian surface and moves/evolves with the motion of the material (the Li electrode in this case). The boundary conditions imposed on the electrode assume that Li near the top and side faces of the volume V_{Li} exists in a state of hydrostatic pressure p . The justification for this assumption is based on the friction hill analysis [34] that we briefly describe here. A friction hill analysis [34] of the electrode of the symmetric cell considered here (Fig. 2a) shows that there is no slip between the electrode/electrolyte interface over a central region of radius $r_s = R_{\text{Li}}[1 + H_{\text{Li}} \ln(\sqrt{3}\mu_f) / (2\mu_f R_{\text{Li}})]$, where μ_f is the friction co-efficient between the Li and the electrolyte. This is because friction between the electrode and electrolyte builds up hydrostatic pressure from the edge of the electrode so that the central portion is under hydrostatic pressure. For a relatively low value of $\mu_f = 0.2$ and electrode of diameter $2R_{\text{Li}} = 1$ mm and thickness $H_{\text{Li}} = 40$ μm [10], $r_s/R_{\text{Li}} \approx 0.8$ which shows that most of the electrode is under nearly pure hydrostatic pressure. Therefore, following [22] we model free slip on the contacting surfaces of the electrode along the impurity and electrolyte surfaces. Specifically, the imposed boundary conditions on the Eulerian surfaces are given by

$$\begin{aligned} T_i t_i &= 0 \text{ and } T_i n_i = -p && \text{over } r = R \text{ and over } z = H, \\ T_i t_i &= 0 \text{ and } v_i n_i = \frac{j\Omega_{\text{Li}}}{F} && \text{over } r > a \text{ on } z = 0 \text{ (i. e., over } S_e). \end{aligned} \quad (18)$$

Here, t_i and n_i are unit tangential and outward normal vectors to the electrode surfaces with $T_i = \sigma_{ij} n_j$. On the Lagrangian void surface S_v , we impose $T_i = 0$ on the portion not in contact with the impurity (i.e., vacuum or no pressure inside the void as there is no path for atmospheric

air to enter the growing void) and frictionless contact over the portion in contact with impurity surface such that $T_i t_i = 0$ and $v_i n_i = 0$. Recall that, in (18), j over S_e is not known a-priori and requires the coupled solution with the governing equations of the electrolyte.

Finally, we need to specify the loading of the cell. Envisage an external power source (Fig. 2a) connected to the symmetric cell being analysed. The loading due to this power source is specified in terms of the areal current density j_∞ in the cell in the absence of impurity. In this case, the electric field within the electrolyte is one-dimensional with j_∞ related to the electrode potential ϕ_p via

$$j_\infty = \frac{\phi_p}{(L/\kappa + Z_0)}. \quad (19)$$

Since $R \gg a$, the relation

$$I = 2\pi \int_0^R j r dr \approx j_\infty \pi R^2 \quad (20)$$

holds to within 0.005% for all the calculations presented here, i.e., to a very high degree of accuracy the total current is not affected by the presence of the impurity.

2.5 *Material parameters and numerical solution methodology*

All results are presented for an Li/LLZO interface of relatively low resistance which typically implies $2 \Omega\text{cm}^2 \leq Z_0 \leq 20 \Omega\text{cm}^2$ [20]: here we choose a representative value of $Z_0 = 5 \Omega\text{cm}^2$ for all calculations presented in Sections 3 and 4. The material parameters for the LLZO and Li are well-established in the literature and are listed in Table 1. We shall present results for an impurity particle/void of radius a_0 in the range $0.1 \mu\text{m} \leq a_0 \leq 0.5 \mu\text{m}$ and, following Shishvan et al. [22], we will take $a_0 = 0.25 \mu\text{m}$ as the reference value.

Table 1: Summary of material parameters for an Li/LLZO/Li cell.

Material parameter	Symbol	Value	Ref.
Conductivity of LLZO	κ	0.46 mS cm ⁻¹	[20]
Shear modulus of Li metal	G_{Li}	3 GPa	[21]
Magnitude of Burgers vector	b	0.25 nm	[21]
Molar volume of Li	Ω_{Li}	$13.1 \times 10^{-6} \text{ m}^3 \text{ mol}^{-1}$	standard
Enthalpy of vacancy formation in Li	h_{v}	50 kJ mol ⁻¹	[35]
Molar volume of vacancies in Li metal	Ω_{v}	$6 \times 10^{-6} \text{ m}^3 \text{ mol}^{-1}$	[36]
Reference stress for Li metal	σ_0	1 MPa	[27]
Reference strain rate for Li metal	$\dot{\epsilon}_0$	0.01 s ⁻¹	[27]
Critical strain rate for Li metal*	$\dot{\epsilon}_{\text{c}}$	10 ⁻⁵ s ⁻¹	[21]
Power-law exponent for Li metal	n	1/6.6	[27]
Reference interfacial resistance	Z_0	5 Ωcm^2	[20]
Reference Butler-Volmer symmetry factor	β	0.5	standard

* Li metal in [21] has a grain size of 100 μm .

The inclusion of the effect of dislocations on the interfacial flux requires some additional considerations. Consider the case of loading with a current $j_{\infty} = 1 \text{ mA cm}^{-2}$. The strain rate in the vicinity of a $a_0 = 0.25 \mu\text{m}$ impurity particle scales as $\dot{\epsilon} \propto j_{\infty} \Omega_{\text{Li}} / (F a_0)$ and the stress follows from (14) as $\sigma \approx 1 \text{ MPa}$. Consequently, we anticipate a dislocation density $\rho_{\text{d}} \approx 0.3 \mu\text{m}^{-2}$ around the particle with an associated dislocation spacing $1/\sqrt{\rho_{\text{d}}} \approx 1.8 \mu\text{m}$. On the other hand, large gradients in stress will occur over a length $\approx 10a_0 = 2.5 \mu\text{m}$. Recall that the empirical dislocation density relation (15) is inferred from uniaxial tensile experiments and is valid when the spatial variations in σ are small over length scales on the order of the dislocation spacing. Clearly, this requirement is not met for the flow field within the Li around the $a_0 = 0.25 \mu\text{m}$ impurity and thus it is not appropriate to use (15) along with (1) and (2) to estimate Z in a pointwise manner along the interface. To circumvent this issue, Shishvan et al. [22] proposed a scheme whereby a dislocation density averaged over a regularising length scale λ is employed in (2) rather than a pointwise density. This sort of averaging to regularise a local constitutive description has been used extensively to describe mechanical properties; see for example [37-38] and here we shall extend such a scheme to model void growth.

First, consider the interfacial resistance Z_{tip} at the tip $r = a$ of the void along $z = 0$. We assume that Z_{tip} is set by an average dislocation density in the vicinity of the tip and thereby modify (2) so that

$$Z_{\text{tip}} = Z_0 \langle \hat{\theta}_v \rangle^{\beta-1} \exp\left(-\frac{(1-\beta)h_v}{RT}\right), \quad (21)$$

where $\langle \hat{\theta}_v \rangle$ is a volume-averaged fraction of effective vacant sites given by

$$\langle \hat{\theta}_v \rangle = \exp\left(-\frac{h_v}{RT}\right) + \alpha \frac{\Omega_{\text{Li}} b^2}{\Omega_v V} \int_{V_{\text{Li}}} w_\lambda \rho_d dV. \quad (22)$$

Here, w_λ is a weighting function that is introduced to bias $\langle \hat{\theta}_v \rangle$ to depend more significantly on dislocations in the vicinity of the void tip. The regularising length scale λ is introduced through w_λ such that

$$w_\lambda \equiv \frac{\exp[-(d/\lambda)^2]}{\int_{V_{\text{Li}}} \exp[-(d/\lambda)^2] dV}, \quad (23)$$

where d is the radial distance of a material point within the Li electrode measured from the current tip of the void located at $(r, z) = (a, 0)$; see inset of Fig. 2a. Recall that since the dislocation spacings are on the order of the length scales over which the electrode is deforming, we cannot calculate Z in a pointwise manner and hence propose a phenomenological form for the spatial distribution of Z along the interface. Recalling that the reduction in resistance is a maximum at the void tip $(r, z) = (a, 0)$ and that Z will be affected by dislocations over a length that scales with the current void size we specify that Z varies as

$$Z(r) = Z_{\text{tip}} + (Z_0 - Z_{\text{tip}}) \left[1 - \exp\left(-\frac{r-a}{\gamma a}\right)\right], \quad (24)$$

where γ is a non-dimensional parameter that sets the length scale over which dislocations influence the interfacial resistance. Thus, accounting for the effect of dislocations within the electrode adds three new material parameters to the formulation, viz. αk , λ and γ . The parameters αk and λ are calibrated in [22] and here we shall use these values, viz. $\alpha k = 2.7$ and $\lambda = 0.5 \mu\text{m}$. The additional parameter γ is not precisely known via independent measurements and based on some scoping simulations carried out as part of this study we use $\gamma = 4$ for the results presented in the main text and show the sensitivity of the results to the choice of γ in the Supplementary Information.

In all calculations presented subsequently, we use a domain of size $R = L = H = 400a_0$ which is sufficiently large to approximate an isolated impurity in an infinitely large cell. The coupled solutions of the Laplace equation in the electrolyte and nonlinear Stokes flow equations in the electrode were obtained using the Multiphysics software Comsol[®]. As shown in Fig. 2b, a regular mesh is needed in the Li for resolving the flow fields. To maintain the quality of the mesh during the void growth, we employ a feature called “moving mesh” in the Multiphysics software Comsol[®]; see Fig. 2b. With this feature enabled, the solution technique used in the electrode is akin to an Arbitrary Lagrangian-Eulerian (ALE) description which is capable of coping with the large distortion of the Li. Further, to impose contact between the Lagrangian Li surface and the impurity particle, we use the “volume force” interface/feature in the Multiphysics software Comsol[®] which penalizes the penetration of Li into the impurity particle.

3. Predictions of interfacial flux focusing

High flux focussing is a requirement to initiate void growth. Hence, we first discuss predictions of flux focusing to set the context of the void growth results presented in Section 4. All

predictions use the modified Butler-Volmer kinetics which accounts for the decrease in interfacial resistance due to dislocations associated with the creep deformation of the Li electrode. Throughout, time $t = 0$ corresponds to the instant when the stripping current was imposed.

A dimensional analysis provides insight into the dependence of flux focussing on key parameters that include the creep properties of the Li, the impurity size and the imposed stripping current j_∞ . For fixed values of the parameters αk , λ and γ associated with the presence of dislocations, the functional form of the non-dimensional interfacial current at time $t = 0^+$ is

$$\frac{j}{j_\infty} = f \left[\bar{r} \equiv \frac{r}{a_0}, \bar{\sigma}_0 \equiv \left(\frac{\Omega_{\text{Li}}}{FZ_0} \right)^2 \frac{\sigma_0}{\dot{\epsilon}_0 \kappa}, \bar{j}_\infty \equiv \frac{j_\infty \Omega_{\text{Li}}}{F \dot{\epsilon}_0 \kappa Z_0}, \bar{a}_0 \equiv \frac{a_0}{\kappa Z_0} \right], \quad (25)$$

where $j = j_i n_i$ is the interfacial current along the interface with n_i denoting the outward normal to the electrode. We now proceed to explore this dependency of j/j_∞ around both an isolated pre-existing hemispherical void or impurity particle of radius a_0 .

3.1 Low flux focusing on the periphery of pre-existing voids

First consider the case of a pre-existing hemispherical void of radius a_0 . Predictions of the spatial variation of the normalised flux j/j_∞ along the interface at time $t = 0^+$ are shown in Fig. 3a for selected choices of a_0 . A small flux concentration exists at the periphery of the void ($r/a_0 = 1$) with the flux dropping to its far-field value of j_∞ for $r/a_0 > 3$. We define the flux concentration factor as $K_j = \max(j)/j_\infty$ and include predictions of K_j as a function of a_0 in Fig. 3b. Over the entire range of void sizes investigated here $K_j \approx 1$ which implies spatially uniform stripping with minimal deformation of the Li electrode. Under these conditions, the void is expected to shrink rather than grow (this is shown explicitly in Section 4.1). Thus,

stripping in the presence of a pre-existing void occurs without creep deformation and therefore the strain rate and stress fields within the electrode almost vanish. We can therefore set $\dot{\epsilon}_0 \rightarrow \infty$ and the functional dependence (25) of j upon the independent non-dimensional groups reduces to $j/j_\infty = f[\bar{r}, \bar{a}_0]$. Consequently, flux focussing predictions presented in Fig. 3 are independent of the creep properties of the Li and the imposed stripping current j_∞ . We note in passing that since there is no creep deformation of the electrode around a pre-existing void and hence no generation of dislocations within the electrode, standard Butler-Volmer kinetics adequately describes the interface flux in this case.

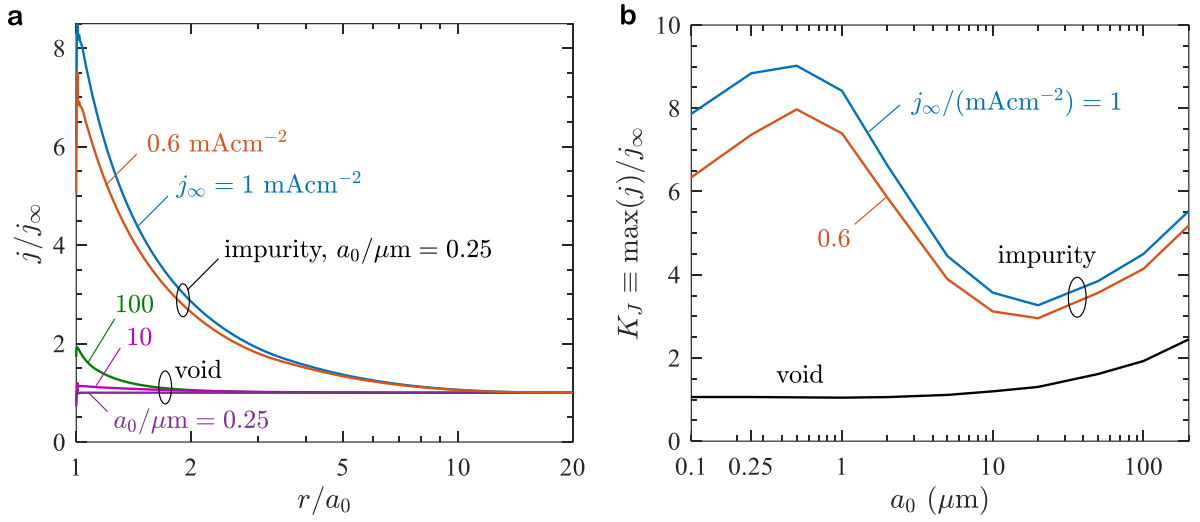


Figure 3: (a) Spatial distribution of the normalised flux j/j_∞ over the interface at time $t = 0^+$ for three initial sizes a_0 of a pre-existing hemispherical void at the interface and a hemispherical impurity of size $a_0 = 0.25 \mu\text{m}$. (b) The corresponding flux concentration factor K_J as a function of a_0 for impurity particles and pre-existing voids. The normalised fluxes for a pre-existing void are insensitive to the current j_∞ but are strongly influenced by j_∞ for the impurity.

3.2. High flux focusing on the periphery of impurities on the interface

The presence of dislocations enhances the flux focussing by reducing the interfacial resistance, but dislocations are only generated when the Li deforms, i.e., a spatially non-uniform velocity field is required to exist within the Li. One scenario where a spatially non-uniform velocity

field is inevitable is when an impurity particle is present on the interface as shown in Fig. 2a: flux across the interface is prevented by the impurity and compatibility of deformation implies that Li needs to flow over the impurity particle surface. This spatially inhomogeneous flow will induce deformation within the Li and thereby generate dislocations. To address this, we proceed to analyse the case of a hemispherical solid impurity particle of radius a_0 on the interface.

Predictions of the normalised flux j/j_∞ over the interface at time $t = 0^+$ are also shown in Fig. 3a for an impurity of size $a_0 = 0.25 \mu\text{m}$ and imposed currents $j_\infty = 1 \text{ mAcm}^{-2}$ and 0.6 mAcm^{-2} . These results are markedly different from that for a pre-existing void in two important ways: (i) the flux concentration around the periphery is much higher such that $K_j \approx 8.5$ for the impurity particle while $K_j \approx 1$ for the same size of a pre-existing void, and (ii) significant stresses are generated in the Li electrode and consequently the normalised interfacial fluxes are now dependent on j_∞ in line with the full dependence shown in (25). The dependence of flux concentration factor K_j upon impurity size a_0 is included in Fig. 3b for two values of j_∞ . The variation of K_j with a_0 is very similar for two values of j_∞ and additionally, K_j increases with increasing j_∞ . Intriguingly, in contrast to the case of a pre-existing void, K_j for an impurity particle varies non-monotonically with increasing a_0 .

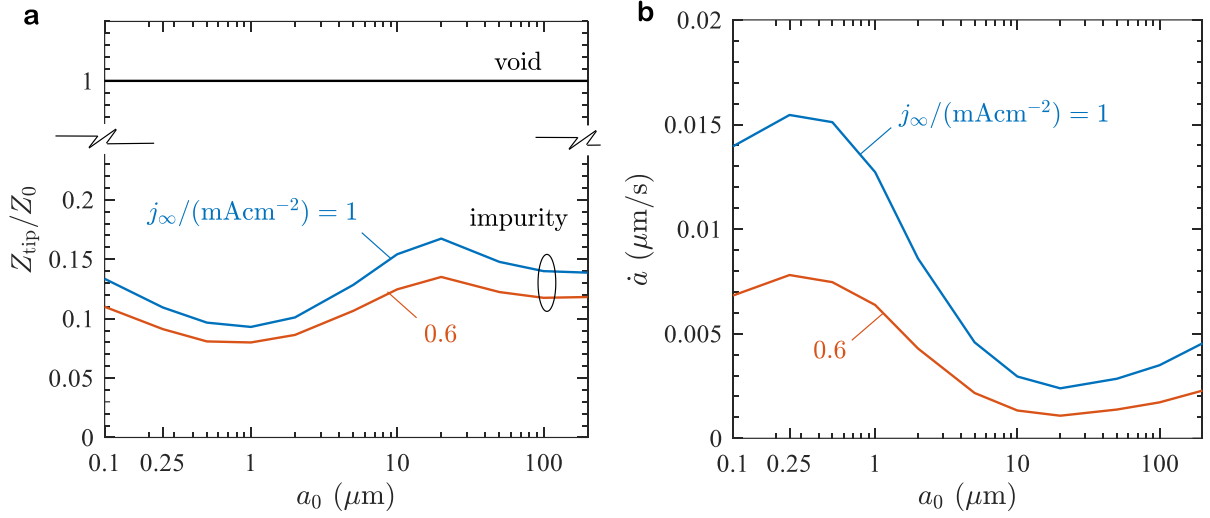


Figure 4: (a) The variation in Z_{tip} with impurity particle radius a_0 at time $t = 0^+$ and (b) the corresponding velocity \dot{a} of the growth of the void along the interface at time $t = 0^+$. Results are shown for two choices of the stripping current j_∞ . In (a) we also show the case of the void where $Z_{\text{tip}}/Z_0 = 1$ over the whole range of a_0 values investigated here.

The source of this rather counterintuitive behaviour can be traced to Z_{tip} . Predictions of the initial ($t = 0^+$) normalised tip interfacial resistance Z_{tip}/Z_0 as a function of a_0 are given in Fig. 4a. While Z_{tip} equals Z_0 for a pre-existing void, Z_{tip} is much less than Z_0 for an impurity particle on the interface. This decrease in interfacial resistance around the periphery of the impurity particle is the source of the high flux concentration when an impurity particle is present – a lower Z_{tip} value implies a higher interfacial flux for the same overpotential across the interface. The non-monotonic variation of K_J with a_0 (Fig. 3b) is also mirrored in Z_{tip} (Fig. 4a) and both the reduction in Z_{tip} compared to Z_0 and the non-monotonic variation can be understood by considering the stress (and dislocation density) in the vicinity of the impurity particle. The spatial variation of the normalised von-Mises stress σ/σ_0 in the Li around the impurity at $t = 0^+$ for impurity particles of radii $a_0 = 0.1 \mu\text{m}$, $0.5 \mu\text{m}$ and $10 \mu\text{m}$ is included in Fig. 5 (for an imposed current $j_\infty = 1 \text{ mAcm}^{-2}$). Large stresses develop in the vicinity of

the impurity particle and are associated with spatial gradients in the velocity field: the flow of Li around the impurity results in a strain rate in the vicinity of the impurity particle that scales as $j_{\infty}\Omega_{\text{Li}}/(Fa_0)$ and thus, the strain rates (and stresses) decrease with increasing a_0 . However, the region over which these large stresses persist also scales with a_0 and this implies that while the stresses increase with decreasing a_0 these stresses are increasingly localised over smaller volumes. These stresses within the Li (which in turn set the dislocation density distributions – see dual colour bar scale in Fig. 5) explain the high values of K_J and the corresponding non-monotonic variation in K_J with a_0 as follows:

- (i) The high stresses around the impurity lead to a high dislocation density ρ_d (Fig. 5) which in turn reduces Z_{tip} , see (21) and (22).
- (ii) High stresses and high dislocation densities exist over a region of size $\sim a_0$ around the impurity. On the other hand, the volume-averaged dislocation density in (22) that sets Z_{tip} is calculated by averaging over a length scale $\lambda = 0.5 \mu\text{m}$. Thus, the average dislocation density is low in the $a_0 = 0.1 \mu\text{m}$ case as the averaging region is larger than the region over which the high stresses exist; see Fig. 5a. With increasing a_0 the stresses are high over a larger portion of the averaging region (Fig. 5b) and thus Z_{tip} decreases and K_J increases. This continues until $a_0 \approx \lambda$.
- (iii) For $a_0 > \lambda$, deformation occurs over the entire averaging volume, but the strain rates which scale as $j_{\infty}\Omega_{\text{Li}}/(Fa_0)$ decrease with increasing a_0 . Thus, the dislocation densities are lower and therefore Z_{tip} increases (Fig. 4a) and K_J decreases (Fig. 3b) with increasing $a_0 > \lambda$.
- (iv) For impurity sizes $a_0 > 10 \mu\text{m}$ (Fig. 5c), the flux concentration factor K_J again starts to increase with increasing a_0 (Fig. 3b). This is surprising as the above arguments suggest that for $a_0 > \lambda$, K_J should continue to decrease with increasing

a_0 . However, another effect comes into play. Flux concentrations due to inhomogeneity in the electric field within the electrolyte increase as the material length scale κZ_0 becomes on the order of the impurity sizes a_0 . For $a_0 > 10 \mu\text{m}$, $\bar{a} \equiv a_0/(\kappa Z_0) > 0.5$ and the flux concentration due to the electric field within the electrolyte becomes significant. This effect combines with the elevation in dislocation density due to flow of Li in the electrode around the impurity to increase K_J with increasing a_0 for $a_0 > 10 \mu\text{m}$.

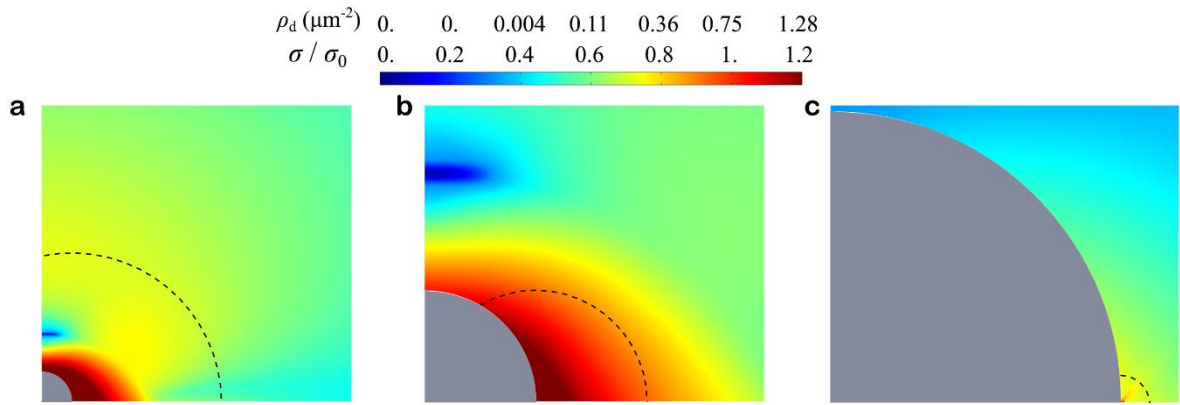


Figure 5: Predictions of the distribution of the normalised von-Mises stress σ/σ_0 around the (a) $a_0 = 0.1 \mu\text{m}$, (b) $a_0 = 0.5 \mu\text{m}$ and (c) $a_0 = 10 \mu\text{m}$ impurity particle at time $t = 0^+$ for a stripping current $j_\infty = 1 \text{ mAcm}^{-2}$. We show a region (dashed line) of radius $\lambda = 0.5 \mu\text{m}$ centred at the tip of the impurity (shaded grey) along the interface to indicate the region over which the dislocation density is averaged. Recalling that the dislocation density is directly related to σ via Eq. (15) we include a non-linear dual scale to indicate the spatial distribution of the dislocation density ρ_d .

The high flux concentration around the periphery of the impurity (i.e., high K_J value) is commonly assumed to result in void growth [15]. For the low values of K_J associated with a pre-existing void (Fig. 3), we show in Section 4.1 that the void shrinks over the full range of void sizes considered here. On the other hand, an impurity particle on the interface results in a high K_J value and we expect voids to initiate under these circumstances. The initiation of void

growth occurs at the periphery of the impurity along the electrode/electrolyte interface (i.e., at $(r, z) = (a_0, 0)$) and we give predictions of the initial void growth rate \dot{a} along $z = 0$ in Fig. 4b. A positive value of \dot{a} implies the detachment of Li from the impurity at $(r, z) = (a_0, 0)$ and therefore the initiation of void growth commences over the whole range of impurity particle sizes and current densities considered in Fig. 4b. Importantly, the value of \dot{a} is sensitive to the value of K_J such that a higher K_J value results in a higher initial growth rate of a void. Additional exploratory calculations with lower currents j_∞ (not included here for the sake of brevity) suggest that voids do not initiate (i.e., $\dot{a} = 0$) for K_J values less than about 2.5.

4. Analysis of void growth during stripping

We proceed to analyse the temporal evolution of voids at the electrode/electrolyte interface during *stripping* of Li from the electrode. We consider the two cases of isolated hemispherical imperfections on the electrode/electrolyte interface discussed in Section 3: (i) a pre-existing void and (ii) a rigid impurity particle.

4.1. Pre-existing voids shrink during stripping

First consider the case of the isolated pre-existing hemispherical void of radius $a_0 = 0.25 \mu\text{m}$. Predictions of the time-evolution of void shape are given in Fig. 6 at three selected times for the cell subjected to a current density $j_\infty = 0.5 \text{ mA cm}^{-2}$ (see also Supplementary video S1). This figure also includes the spatial distribution of normalised flux j_z/j_∞ in the electrolyte, where j_z is the flux in the z –direction, and the spatial distribution of normalised von-Mises stress σ/σ_0 within the electrode. It is clear from the snapshots in Fig. 6 that the void shrinks (i.e., radius of the void decreases along $z = 0$ and reduces in volume) under stripping conditions. This occurs with negligible deformation of the Li as is evident by observing that the stresses (and consequently strain rates) within the Li are small as anticipated from the flux

focussing predictions of Fig. 3. To further illustrate that stripping occurs with negligible deformation of the electrode, we include contours of the Stokes stream function ψ within the electrode. These surfaces are placed such that the difference in value of the stream function $\Delta\psi$ between consecutive surfaces is constant and given by $\Delta\bar{\psi} \equiv \Delta\psi F / (j_\infty \Omega_{\text{Li}} a_0^2) = 0.5$ so that the volumetric flow rate of the Li between consecutive surfaces equals $Q = 2\pi\Delta\psi = \pi(j_\infty \Omega_{\text{Li}} a_0^2) / F$. The contours are almost vertical: recalling that the material velocities are parallel to the stream function contours, void shrinkage occurs with Li being uniformly stripped over the electrode/electrolyte interface S_e .

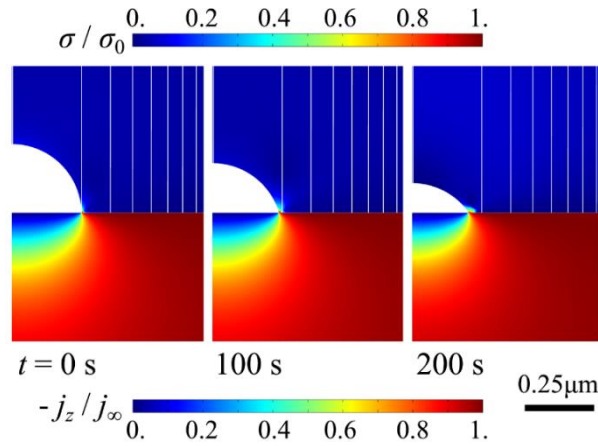


Figure 6: Snapshots showing the evolution of a pre-existing hemispherical void of radius $a_0 = 0.25 \mu\text{m}$ on the electrode/electrolyte interface with a stripping current $j_\infty = 0.5 \text{ mAcm}^{-2}$ (see also Supplementary Video S1). We include contours of the normalised von-Mises stress σ/σ_0 in the Li and the flux j_z/j_∞ in the electrolyte. Contour surfaces of equally spaced Stokes stream functions (with $\Delta\bar{\psi} = 0.5$) are also shown to indicate the flow of the Li and the associated velocity gradients.

4.2. Void growth occurs around an impurity particle on the interface

Pre-existing voids on the electrode/electrolyte interface shrink but the flux focussing results of Section 3 indicate that void growth is expected to initiate around a hemispherical impurity particle on the electrode/electrolyte interface. We thus proceed to investigate temporal

evolution of void growth around an isolated hemispherical impurity both in the absence of and with an imposed stack pressure.

4.2.1. Predictions in the absence of stack pressure

Two distinct regimes of void growth are observed, depending upon the combination of imposed current and impurity size. We consider each of them in turn. First, consider the case of a high current with $j_\infty = 1 \text{ mA cm}^{-2}$ and $a_0 = 0.25 \text{ }\mu\text{m}$. The temporal evolution of the growth of a void around the impurity is shown in Fig. 7 and Supplementary Video S2 with contours of normalised von-Mises stress σ/σ_0 and normalised flux j_z/j_∞ shown in the Li and electrolyte, respectively. Contour surfaces of the Stokes stream function ψ , spaced at $\Delta\bar{\psi} \equiv \Delta\psi F/(j_\infty \Omega_{\text{Li}} a_0^2) = 10$, are included within the electrode to illustrate the flow of Li. Two phases of growth of the void are observed. Initially, the void grows along the electrode/electrolyte interface but without growing in height until $t \approx 400 \text{ s}$: the void evolves to a pancake-like shape, as observed experimentally [10]. The contours of Stokes stream function curve over the surface of this growing void consistent with the void growing in the r –direction. At $t \approx 400 \text{ s}$, the void along the electrode/electrolyte interface has attained a radius $a \approx 4 \text{ }\mu\text{m}$ and the void then begins to collapse, i.e., its volume reduces as its height shrinks but there is negligible reduction in the radius a (Fig. 7). To understand this, recall that the high flux concentration around the periphery of the void causes the void to grow while the overall stripping flux j_∞ tends to close the void. While the normalised void radius a/a_0 remains relatively small ($a/a_0 < 16$ in this case), the mechanical support provided by the impurity particle combined with the high flux concentration is sufficient for the void to grow and not collapse. For $a/a_0 \geq 16$, the dislocation density remains high on the void periphery (see dual colour bar scale in Fig. 7) and consequently there continues to be high flux focussing. However, the central mechanical support provided by the impurity particle is insufficient for this

relatively large void and the void begins to collapse under the high stripping flux of $j_\infty = 1 \text{ mA cm}^{-2}$.

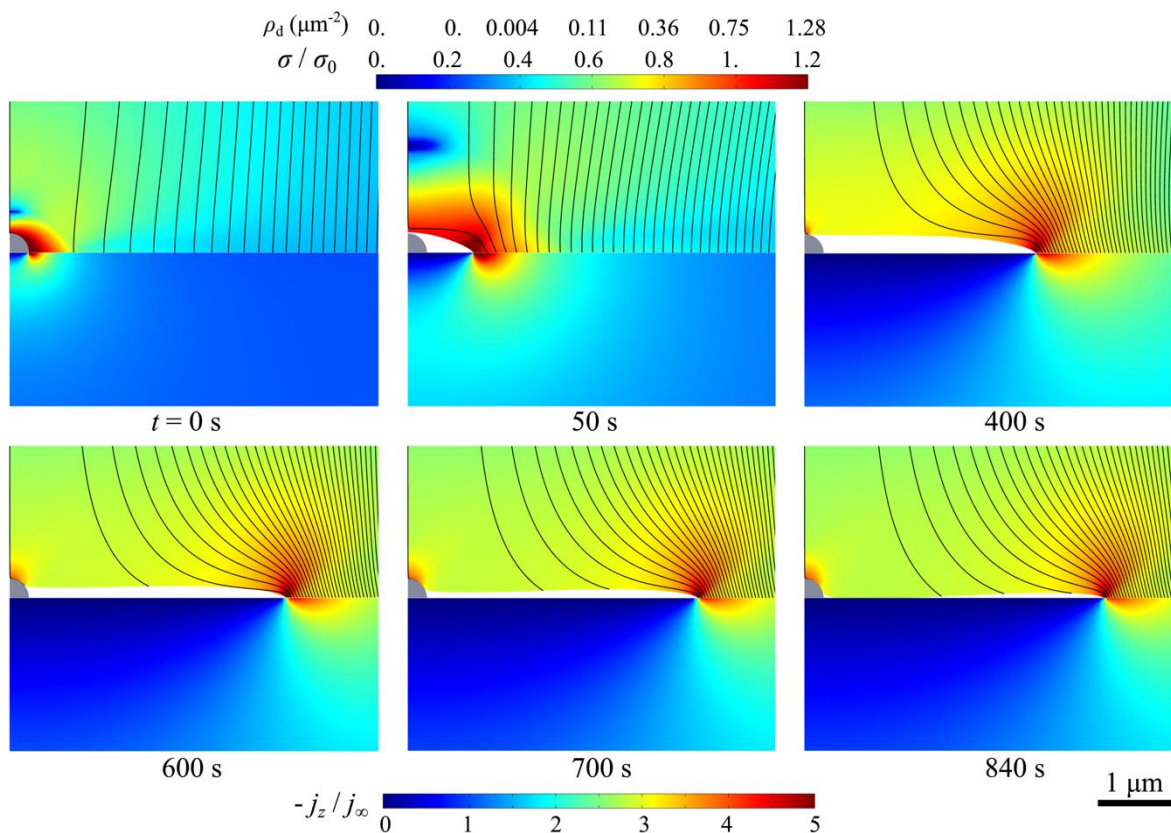


Figure 7: Temporal evolution of void for evolving around an $a_0 = 0.25 \mu\text{m}$ impurity particle with an imposed stripping current $j_\infty = 1 \text{ mA cm}^{-2}$ (see also Supplementary Video S2). We include contours of the normalised von-Mises stress σ/σ_0 in the Li and the flux j_z/j_∞ in the electrolyte. Contour surfaces of equally spaced Stokes stream functions (with $\Delta\bar{\psi} = 10$) are also shown to indicate the flow of the Li and the associated velocity gradients. Recalling that the dislocation density is directly related to σ via Eq. (15) we include a non-linear dual scale to indicate the spatial distribution of the dislocation density ρ_d .

Now consider the case of a low stripping current $j_\infty = 0.4 \text{ mA cm}^{-2}$ again with an isolated $a_0 = 0.25 \mu\text{m}$ impurity on the interface. The temporal evolution of the Li around the impurity and the associated flux within the electrolyte are illustrated in Fig. 8 in a manner analogous to Fig. 7. A void initiates from the surface of the impurity and grows along the interface without

growing in height, i.e., it assumes a pancake shape. However, void growth is now less with the void attaining a maximum radius $a \approx 1.5 \mu\text{m}$. More intriguingly, this void, unlike the $j_\infty = 1.0 \text{ mA cm}^{-2}$ case, does not collapse but stabilises at the state shown at $t = 1800 \text{ s}$ in Fig. 8 (see also Supplementary Video S3). We rationalise this by noting that the lower current implies a lower K_j and thus the void does not grow to the extent seen in Fig. 7. This smaller void is mechanically supported by the impurity, and a balance is attained between the flux concentration at the void periphery that tends to grow the void and the overall stripping current j_∞ that tends to collapse the void. We emphasise that the stable voids are much smaller than those observed in experiments [10].

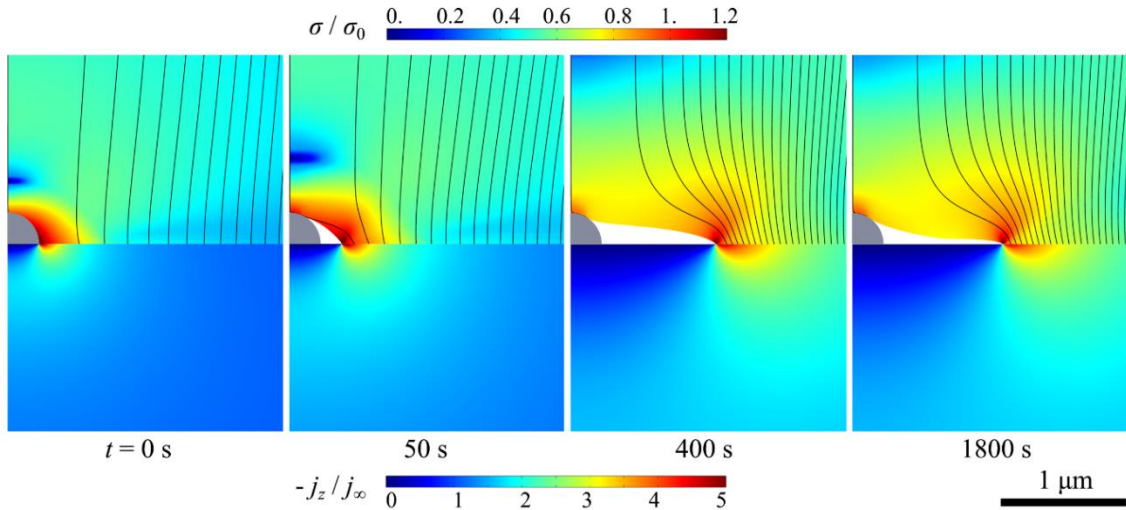


Figure 8: Temporal evolution of void for evolving around an $a_0 = 0.25 \mu\text{m}$ impurity particle with an imposed stripping current $j_\infty = 0.4 \text{ mA cm}^{-2}$ (see also Supplementary Video S3). We include contours of the normalised von-Mises stress σ/σ_0 in the Li and the flux j_z/j_∞ in the electrolyte. Contour surfaces of equally spaced Stokes stream functions (with $\Delta\bar{\psi} = 4$) are also shown to indicate the flow of the Li and the associated velocity gradients.

The results for calculations over a range of stripping currents and impurity particles sizes are summarised in Fig. 9a in terms of the maximum radius $a_{\text{max}} - a_0$ of the void along the electrode/electrolyte interface as a function of j_∞ . Here, a_{max} is defined as either the maximum

radius of the stable void (Fig. 8 and Supplementary Video S3) or the maximum radius that the void attains before it collapses (Fig. 7 and Supplementary Video S2). Stable void radii in Fig. 9a are marked with filled symbols while an open symbol indicates a collapsing void. Clearly, the regime of behaviour is dependent on both a_0 and j_∞ and we illustrate this via the map in Fig. 9b using axes of a_0 and j_∞ . The map shows that for a given impurity size, stable voids form at low currents but voids collapse at higher currents and the transition current density j_T increases with increasing a_0 .

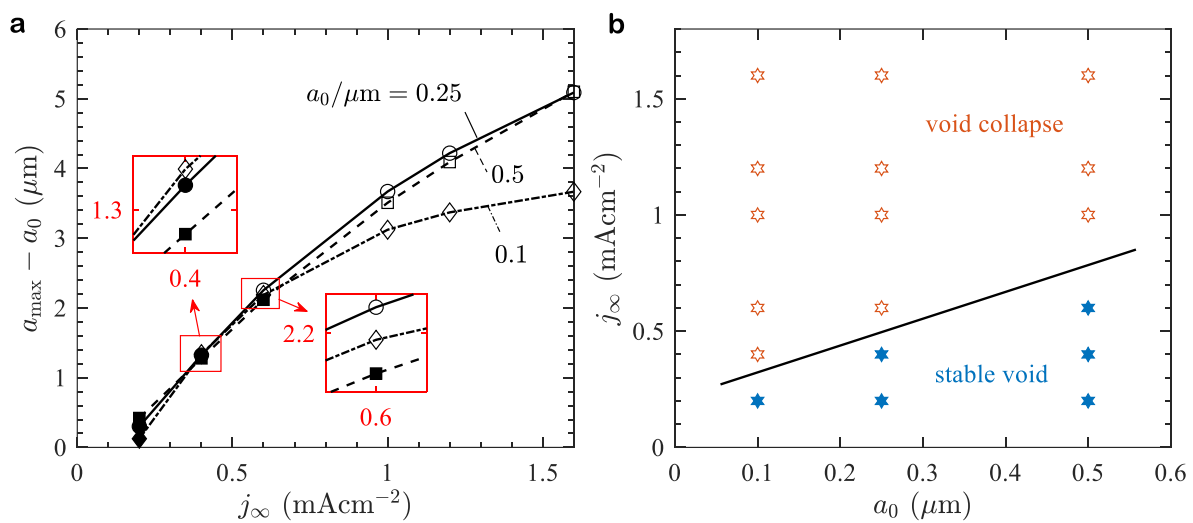


Figure 9: (a) Predictions of the maximum radius a_{\max} that a void growing around an impurity particle of radius a_0 attains before it either collapses or attains a stable shape as a function of the stripping current j_∞ . Here a_{\max} is measured along the electrode/electrolyte interface and results shown for selected choices of the impurity size a_0 . We plot the results in terms of $a_{\max} - a_0$ to allow for easy comparison across the different impurity particle sizes. The open and filled symbols indicate a collapsing and stable void, respectively. (b) A map using axes of a_0 and j_∞ to show the regimes where voids collapse or attain stable shapes.

4.2.2. Effect of an imposed stack pressure

The imposition of a stack pressure p (Fig. 2a) is known to suppress the formation of voids at the electrode/electrolyte interface [10, 13]. Here, we analyse the effect of stack pressure p via

the boundary conditions detailed in Section 2.4 where the central portion of the electrode is under an overall state of hydrostatic pressure p .

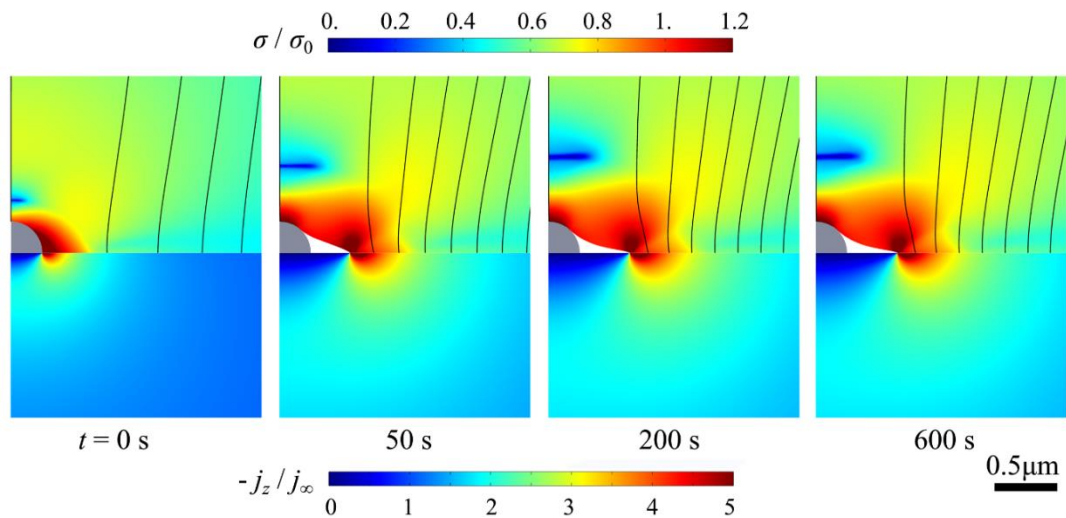


Figure 10: Temporal evolution of void for evolving around an $a_0 = 0.25 \mu\text{m}$ impurity particle with an imposed stripping current $j_\infty = 1 \text{ mA cm}^{-2}$ for a cell subjected to a stack pressure $p = 1 \text{ MPa}$ (see also Supplementary Video S4). We include contours of the normalised von-Mises stress σ/σ_0 in the Li and the flux j_z/j_∞ in the electrolyte. Contour surfaces of equally spaced Stokes stream functions (with $\Delta\bar{\psi} = 10$) are also shown to indicate the flow of the Li and the associated velocity gradients.

The temporal evolution of the void growing around the $a_0 = 0.25 \mu\text{m}$ impurity is shown in Fig. 10 for the choice $j_\infty = 1 \text{ mAcm}^{-2}$ and a stack pressure $p = 1 \text{ MPa}$ (see also Supplementary Video S4). The void grows to $a \approx 0.5 \mu\text{m}$ and then stabilises. By contrast, in the absence of a stack pressure the void grows to $a \approx 4 \mu\text{m}$ and then collapses (Fig. 7). The imposed pressure suppresses void growth, and consequently the void remains sufficiently supported by the impurity particle preventing void collapse. Predictions of the temporal evolution of the void radius $a - a_0$ along the electrode/electrolyte interface for $j_\infty = 1 \text{ mAcm}^{-2}$ at selected stack pressures p are shown in Fig. 11a. Results are presented for voids growing from $a_0 = 0.25 \mu\text{m}$ and $0.5 \mu\text{m}$ impurity particles: as anticipated, void growth is reduced with increasing p . This is summarised in Fig. 11b where we include predictions of the

maximum radius $a_{\max} - a_0$ of a void growing from the $a_0 = 0.25 \mu\text{m}$ impurity as a function of p for two imposed currents j_∞ . The maximum void radius increases with increasing current and over the range of pressures and currents in Fig. 11, we again observe two regimes of behaviour, (i) void collapse, and (ii) formation of a stable void. The behaviour transitions from void collapse at low pressures to the formation of a stable void at larger pressures (the open and filled symbols in Fig. 11b indicate collapsing and stable voids, respectively). This behaviour is summarised in a map in Fig. 12 with axes of p and j_∞ : for $p \geq 1 \text{ MPa}$, a stable void forms for all currents investigated here while in the absence of superimposed pressure a stable void only forms for $j_\infty < 0.5 \text{ mAcm}^{-2}$.

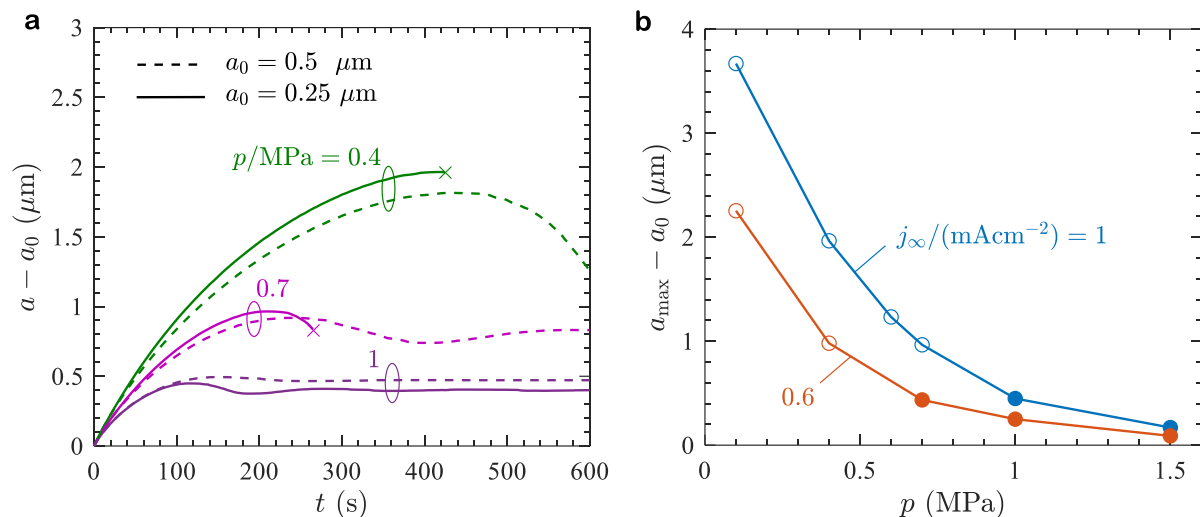


Figure 11: (a) Temporal evolution of the radius a of the void measured along the electrode/electrolyte interface for a stripping current $j_\infty = 1 \text{ mA cm}^{-2}$ and two choices of the impurity particle radius a_0 and selected imposed stack pressures p . The curves that end with a cross indicate that the void collapsed onto the interface at this instant. (b) Predictions of the maximum radius a_{\max} that the void growing around an impurity particle of radius a_0 attains before it either collapses or attains a stable shape as a function of the stack pressure p . Here a_{\max} is measured along the electrode/electrolyte interface. Consistent with Fig. 9, we plot the void size as $a_{\max} - a_0$ and show results for two choices of the stripping current j_∞ for an impurity particle of size $a_0 = 0.25 \mu\text{m}$. The open and filled symbols indicate a collapsing and stable void, respectively.

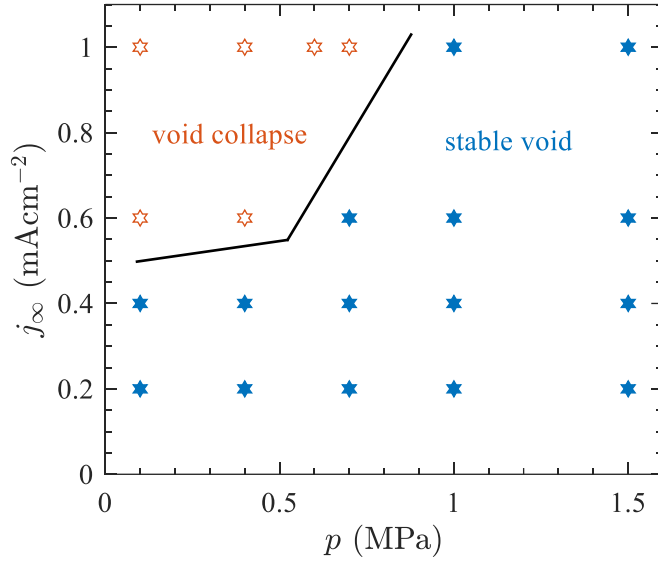


Figure 12: A map using axes of the stack pressure p and stripping current j_{∞} to show the regimes where voids collapse or assume a stable shape around an impurity of size $a_0 = 0.25 \mu\text{m}$.

5. A hypothesis for cell failure by void coalescence

Our calculations show that while pre-existing voids shrink, voids grow around impurity particles on the electrode/electrolyte interface. However, these voids grow to radii of no more than $\sim 10 \mu\text{m}$ before they either collapse or stabilise and thus these isolated voids cannot give rise to the measured precipitous increase in cell voltage during stripping. We hypothesise that the observed failure is a consequence of the coalescence of voids and proceed to discuss this mechanism in the context of our isolated void simulations presented above.

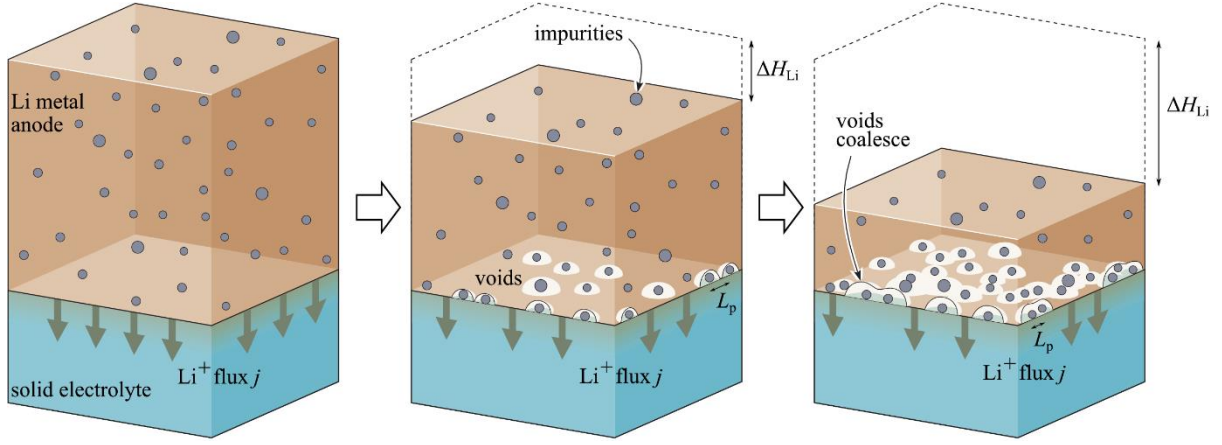


Figure 13: Sketches of impurity particles present in the Li electrode being deposited on the electrode/electrolyte interface during stripping, and the growth of a large void that is supported at multiple locations by these deposited impurity particles.

The impurity particles on the interface can either pre-exist or be deposited on the interface from within the stripping Li electrode as illustrated in Fig. 13. Continued stripping results in an increasing density of impurity particles on the interface with voids growing around each of these impurities. Failure of the cell (i.e., precipitous increase in voltage to maintain the imposed cell current) will occur when voids growing around each of these impurity particles coalesce. Let f denote the volume fraction of spherical impurities particles of radius a_0 within the Li electrode. After stripping for a time t with a current j_∞ , a height $\Delta H_{\text{Li}} = j_\infty t \Omega_{\text{Li}} / F$ of Li has been stripped from the electrode (Fig. 13). All impurities within the stripped portion of the electrode are deposited on the interface. Assuming that these impurity particles are uniformly distributed over the interface, their spacing L_p after a time t of stripping is then given by

$$L_p \approx \sqrt{\frac{F a_0^3}{f j_\infty t \Omega_{\text{Li}}}}. \quad (26)$$

Cell failure by void coalescence occurs at a time $t = t_f$ when this impurity spacing is related to the maximum void radius via $L_p = 2a_{\text{max}}$. It then follows that cell failure occurs after a critical stripping $C_{\text{crit}} = j_\infty t_f$ obtained from (26) as

$$C_{\text{crit}} \approx \frac{F a_0^3}{4f a_{\text{max}}^2}. \quad (27)$$

Recall that a_{max} is a function of j_∞ and the stack pressure p (see for example Fig. 11b) and therefore (27) predicts that the critical stripping capacity at which battery failure occurs also depends on (j_∞, p) .

Predictions of C_{crit} as a function of the stack pressure p are included in Fig. 14a for two choices of j_∞ and our reference set of parameters with $a_0 = 0.25 \mu\text{m}$ and a volume fraction $f = 0.01\%$ of impurities. In qualitative agreement with measurements, the tendency for cell failure decreases (i.e., critical stripping capacity C_{crit} increases) with increasing stack pressure for a given current and with decreasing current for a given stack pressure. Measurements of cell failure are typically conducted by imposing a constant current j_∞ and then gradually decreasing the imposed stack pressure until failure due to a precipitous voltage increase occurs [10-13]. From these measurements, we can extract the time t_f of failure when failure occurs at the stack pressure p . Measurement of $(C_{\text{crit}} \equiv j_\infty t_f, p)$ from [12] is included in Fig. 14a and clearly shows that the model grossly overpredicts the measured critical stripping capacity. Specifically, at an imposed pressure $p = 0.1 \text{ MPa}$ the predictions suggest $C_{\text{crit}} \approx 1 \text{ mAhcm}^{-2}$ for a current $j_\infty = 0.6 \text{ mAcm}^{-2}$ while the measurements show that a current as low as $j_\infty = 0.1 \text{ mAcm}^{-2}$ results in failure at $C_{\text{crit}} \approx 1 \text{ mAhcm}^{-2}$.

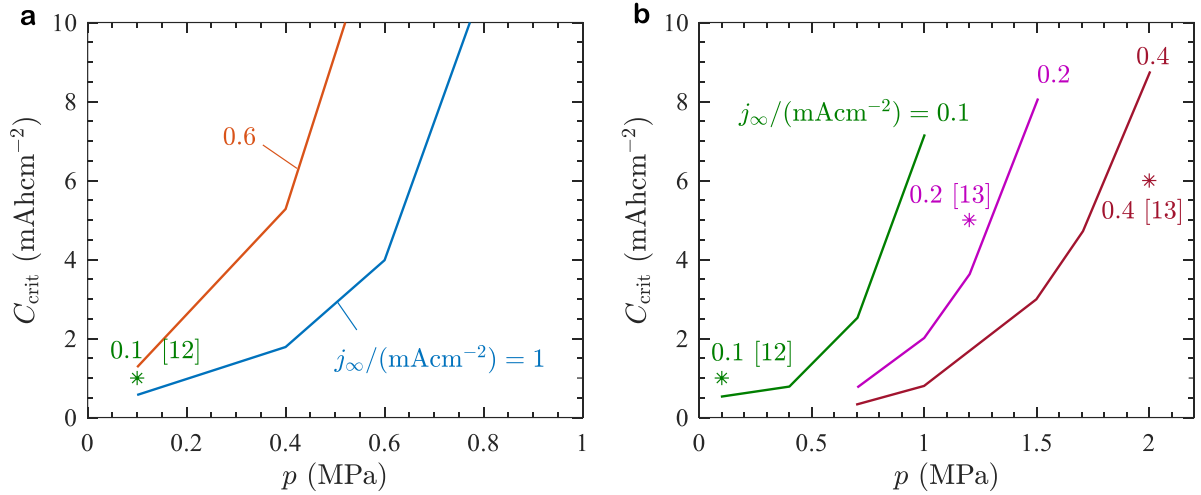


Figure 14: Comparison between predictions and measurements [12, 13] of cell failure by the coalescence of voids growing around impurity particles being deposited on the interface as depicted in Fig. 13. Predictions using (a) reference parameters and (b) modified parameters with $Z_0 = 20 \Omega \text{cm}^2$ and $\beta = 0$. All predictions use spherical impurity particles of radius $a_0 = 0.25 \mu\text{m}$ and a volume fraction $f = 0.01\%$ of impurities. The imposed currents j_{∞} in mA cm^{-2} and the associated reference (within square brackets) for the experimental data points are indicated in each case.

We attributed this discrepancy between predictions and measurements to uncertainties of the model parameters and therefore performed an extensive parametric study to examine the sensitivity of the predictions to key parameters. This study revealed that increasing the interface resistance to $Z_0 = 20 \Omega \text{cm}^2$ and employing a reduced Butler-Volmer symmetry factor of $\beta = 0$ bring the predictions more in line with the measurements. Predictions with these modified parameters (Fig. 14b) show excellent agreement with measurements not only from Ref. [12] but also from Ref. [13] that employed a higher stack pressure. It is worth emphasizing that it generally known that a higher electrode/electrolyte interface resistance increases the propensity of cell failure, and our predictions were brought into agreement with measurements by increasing this interfacial resistance. Thus, while our predictions strongly suggest that the

failure mechanism is the coalescence of voids growing around impurities deposited on the interface, additional experiments are of course required to test this new hypothesis.

6. Concluding discussion

We have investigated the growth of voids at the electrode/electrolyte interface using a framework that couples, via the Onsager formalism, power-law creep deformation of the Li electrode and flux of Li^+ through a single-ion conductor solid electrolyte. The dissipation at the electrode/electrolyte interface is modelled by a modified Butler-Volmer kinetics wherein dislocation-driven creep deformation of the Li electrode leads to a reduction in the interfacial resistance. The dislocation density is set by the deviatoric stresses within the electrode and thus the governing equations for the mechanical fields within the electrode are strongly coupled to the electrochemical fields within the electrolyte and vice-versa.

Pre-existing micron-sized voids along the electrode/electrolyte interface shrink during stripping of the electrode as there is near uniform stripping of Li over the interface. This in turn implies a negligible dislocation density in the electrode and thereby no reduction of interfacial resistance near the void. In contrast, when an impurity particle is present on the interface, the impurity blocks the Li flux and enforces a non-uniform velocity field (i.e., deformation) of the electrode. This deformation and consequent increase in the dislocation density result in a large flux concentration around the periphery of the impurity particle which induces the initiation and growth of a void around the impurity particle. Two regimes of void growth are predicted: (i) at low stripping currents and impurity particle sizes, small and stable voids form and (ii) at high currents or larger impurity particle sizes, larger voids form but these voids ultimately collapse as the impurity particle provides insufficient structural support to keep large voids open. The imposition of a stack pressure typically tends to reduce the void size with these

smaller voids being stable. Nevertheless, for impurity particles on the order of a micron or less, *isolated* voids grow to no greater than 10 μm in size which is substantially smaller than the observed 100 μm or so void sizes.

While the physics which allows for isolated voids to grow to large sizes (e.g., $> 100 \mu\text{m}$) is unclear, we hypothesized that cell failure occurs by the coalescence of voids that grow around impurity particles deposited on the interface from within the stripping Li electrode. These predictions suggest that cell failure is not only dependent on the imposed stack pressure and cell current but also depends on the stripping time. The model predictions were shown to be in good agreement with measurements over a range of cell currents and stack pressures. Nevertheless, this is a new hypothesis for cell failure by void coalescence and requires further experimental validation.

Acknowledgements

The authors are grateful for helpful discussions with Profs. Peter Bruce and Clare Grey. NAF acknowledges support by the Faraday Institution [Solbat, grant number FIRG007].

References

- [1] E. Linden, T.B. Reddy, Handbook of Batteries, 2001, McGraw-Hill: New York.
- [2] P.G. Bruce, S.A. Freunberger, L.J. Hardwick, J.M. Tarascon, Li-O₂ and Li-S batteries with high energy storage, *Nat. Mater.* 2012, **11**, 19-29.
- [3] L. Gireaud, S. Grugeon, S. Laruelle, B. Yriex, J.-M. Tarascon, Lithium metal stripping/plating mechanisms studies: A metallurgical approach, *Electrochem. Commun.* 2006, **8**, 1639-1649.
- [4] K.J. Harry, D.T. Hallinan, D.Y. Parkinson, A.A. MacDowell, Detection of subsurface structures underneath dendrites formed on cycled lithium metal electrodes, *Nat. Mater.* 2014, **13**, 69-73.

- [5] K.J. Harry, X. Liao, D.Y. Parkinson, A.M. Minor, N.P. Balsara, Electrochemical deposition and stripping behavior of lithium metal across a rigid block copolymer electrolyte membrane, *J. Electrochem. Soc.* 2015, **162**, A2699-A2706.
- [6] A. Hooper, B.C. Tofield, All-solid-state batteries, *J. Power Sources* 1984, **11**, 33-41.
- [7] K. Takada, Progress and prospective of solid-state lithium batteries, *Acta Mater.* 2013, **61**, 759-770.
- [8] A. Sharafi, H.M. Meyer, J. Nanda, J. Wolfenstine, J. Sakamoto, Characterizing the Li–Li₇La₃Zr₂O₁₂ interface stability and kinetics as a function of temperature and current density, *J. Power Sources* 2016, **302**, 135-139.
- [9] R.D. Schmidt, J. Sakamoto, In-situ, non-destructive acoustic characterization of solid-state electrolyte cells, *J. Power Sources* 2016, **324**, 126–133.
- [10] J. Kasemchainan, S. Zekoll, D.S. Jolly, Z. Ning, G.O. Hartley, J. Marrow, P.G. Bruce, Critical stripping current leads to dendrite formation on plating in lithium anode solid electrolyte cells, *Nat. Mater.* 2019,**18**, 1105-1111.
- [11] J.D. Spencer, Z. Ning, J.E. Darnbrough, J. Kasemchainan, G.O. Hartley, P. Adamson, D.E. Armstrong, J. Marrow, P. G. Bruce, Sodium/Na β" alumina interface: effect of pressure on voids, *ACS Appl. Mater. Interfaces* 2020, **12**, 678–685.
- [12] T. Krauskopf, H. Hartmann, W.G. Zeier, J. Janek, Toward a fundamental understanding of the lithium metal anode in solid-state batteries - An electrochemo-mechanical study on the garnet-type solid electrolyte Li_{6.25}Al_{0.25}La₃Zr₂O₁₂, *ACS Appl. Mater. Interfaces* 2019, **11**, 14463–4477.
- [13] M.J. Wang, R. Choudhury, J. Sakamoto, Characterizing the Li-solid-electrolyte interface dynamics as a function of stack pressure and current density, *Joule* 2019, **3**, 2165–2178.
- [14] J.D. Spencer, Z. Ning, J.E. Darnbrough, J. Kasemchainan, G.O. Hartley, P. Adamson, D.E. Armstrong, J. Marrow, P. G. Bruce, Sodium/Na β" alumina interface: effect of pressure on voids, *ACS Appl. Mater. Interfaces* 2020, **12**, 678–685.
- [15] Y. Chen, Z. Wang, X. Li, *et al.* Li metal deposition and stripping in a solid-state battery via Coble creep. *Nature* 2020, **578**, 251–255.
- [16] R. Xu, F. Liu, Y. Ye, *et al.* A morphologically stable Li/electrolyte interface for all-solid-state batteries enabled by 3D-micropatterned garnet, *Adv. Mater.* 2021, 2104009.

- [17] Z. Wang, X. Li, Y. Chen *et al.* Creep-enabled 3D solid-state lithium-metal battery, *Chem* 2021, **6**, 2878-2892.
- [18] X. Zhang, Q.J. Wang, K.L. Harrison, S.A. Roberts, S.J. Harris, Pressure-Driven Interface Evolution in Solid- State Lithium Metal Batteries, *Cell Rep. Phys. Sci.* 2020, **1**, 100012.
- [19] U. Roy, N.A. Fleck, V.S. Deshpande, An assessment of a mechanism for void growth in Li anodes, *Extreme Mech. Lett.* 2021, **46**, 101307.
- [20] A. Sharafi, C.G Haslam, R.D. Kerns, J. Wolfenstine, J. Sakamoto, Controlling and correlating the effect of grain size with the mechanical and electrochemical properties of $\text{Li}_7\text{La}_3\text{Zr}_2\text{O}_{12}$ solid-state electrolyte, *J Mater. Chem A* 2017, **5**, 21491.
- [21] P.M. Sargent and M.F. Ashby, Deformation mechanism maps for alkali metals, *Scripta Metall.* 1984, **18**, 145-150.
- [22] S.S. Shishvan, N.A. Fleck, V.S. Deshpande, The initiation of void growth during stripping of Li electrodes in solid electrolyte cells, *J. Power Sources* 2021, **488**, 229437.
- [23] L. Onsager, Reciprocal relations in irreversible processes, I., *Phys. Rev.* 1931, **37**, 405–426.
- [24] L. Onsager, Reciprocal relations in irreversible processes, II., *Phys. Rev.* 1931, **38**, 2265–2279.
- [25] J. Weertman, Dislocation climb theory of steady-state creep, *Trans. Am. Soc. Met.* 1968, **61**, 681-694.
- [26] A. Seeger, P. Haasen, Density changes of crystals containing dislocations, *Phil. Mag. A* 1958, **3:29**, 470-475.
- [27] W.S. LePage, Y. Chen, E. Kazyak, K-H. Chen, A.J. Sanchez, A. Poli, E.M. Arruda, M.D. Thouless, N.P. Dasgupta, Lithium mechanics: Roles of strain rate and temperature and implications for lithium metal batteries *J. Electrochem. Soc.* 2019, **166**, A89.
- [28] M.E. Kassner, M-T. Pérez-Prado, Five-power-law creep in single phase metals and alloys, *Prog. Mater. Sci.* 2000, **45**, 1-102.
- [29] L.A. Feldman, L.C. De Jonghe, Initiation of mode I degradation in sodium-beta alumina electrolytes, *J. Mater. Sci.* 1982, **17**, 517–524.

- [30] L. Porz, T. Swamy, B. W. Sheldon, D. Rettenwander, T. Frömling, H.L. Thaman, S. Berendts, R. Uecker, W. C. Carter, Y.-M. Chiang, Mechanism of Lithium Metal Penetration through Inorganic Solid Electrolytes, *Adv. Energy Mater.* 2017, **7**, 1701003.
- [31] M. Klinsmann, F.E. Hildebrand, M. Ganser, R.M. McMeeking, Dendritic cracking in solid electrolytes driven by lithium insertion, *J. Power Sources* 2019, **422**, 227226.
- [32] S.S. Shishvan, N.A. Fleck, R.M. McMeeking, V.S. Deshpande, Dendrites as climbing dislocations in ceramic electrolytes: Initiation of growth, *J. Power Sources* 2020, **456**, 227989.
- [33] S.S. Shishvan, N.A. Fleck, R.M. McMeeking, V.S. Deshpande, Growth rate of lithium filaments in ceramic electrolytes, *Acta Mater.* 2020, **196**, 444-455.
- [34] G. E. Dieter, *Mechanical Metallurgy*, SI Metric Edition, McGraw-Hill, 1988, pp. 539-549.
- [35] H. Schultz, Defect parameters of bcc metals: group-specific trends, *Mater. Sci. Eng.* 1991, **A141**, 149-167.
- [36] W. Frank, U. Breier, C. Elsässer, M. Fähnle, Properties of monovacancies and self-interstitials in bcc Li: An ab initio pseudopotential study, *Phys. Rev. B* 1993, **48**, 7676.
- [37] Z.P. Bažant, M. Jirásek, Nonlocal integral formulations of plasticity and damage: survey of progress, *J. Eng. Mech.* 2002, **128**, 1119–1149.
- [38] V. Tvergaard, A. Needleman, Effects of nonlocal damage in porous plastic solids, *Int. J. Solids Struct.* 1995, **32**, 1063–1077.

Supplementary Information

Influence of the parameter γ that sets the averaging length scale

The non-dimensional parameter γ sets the length scale over which dislocations influence the interfacial resistance. We have used $\gamma = 4$ in all the calculations in the main body of the paper. To illustrate the influence of γ , we include in Fig. S1 predictions of the temporal evolution of the void radius a along the electrode/electrolyte interface around an $a_0 = 0.25 \mu\text{m}$ impurity particle. Results are shown for $\gamma = 2$ as well as the reference value of $\gamma = 4$. In these calculations, a stripping current $j_\infty = 0.6 \text{ mA cm}^{-2}$ was imposed with no stack pressure and the calculations terminated when the void collapses. While reducing γ results in the formation of a marginally larger void before collapse, the value of γ does not influence the regime of behaviour (i.e., void collapse or formation of a stable void). Moreover, over the full loading range (i.e., imposed current, pressure and impurity size) investigated here, the main conclusion that large voids on the order of $100 \mu\text{m}$ cannot form around isolated micron-sized impurity particles remains unaffected by the choice of γ .

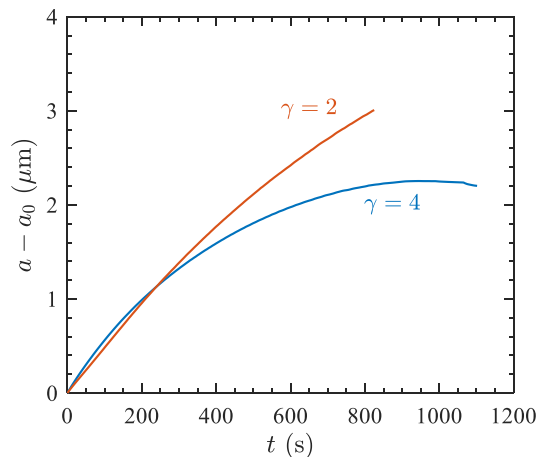


Figure S1: Temporal evolution of the radius a of the void measured along the electrode/electrolyte interface for a stripping current $j_\infty = 0.6 \text{ mA cm}^{-2}$ and two values of the parameter γ (no stack pressure and $a_0 = 0.25 \mu\text{m}$). In both cases the calculations are terminated by the collapse of the void.

Captions for Videos S1 to S4:

Video S1: Temporal evolution of a pre-existing hemispherical void of radius $a_0 = 0.25 \mu\text{m}$ on the electrode/electrolyte interface with a stripping current $j_\infty = 0.5 \text{ mA cm}^{-2}$. No imposed stack pressure.

Video S2: Temporal evolution of void for evolving around an $a_0 = 0.25 \mu\text{m}$ impurity particle with an imposed stripping current $j_\infty = 1 \text{ mA cm}^{-2}$. No imposed stack pressure.

Video S3: Temporal evolution of void for evolving around an $a_0 = 0.25 \mu\text{m}$ impurity particle with an imposed stripping current $j_\infty = 0.4 \text{ mA cm}^{-2}$. No imposed stack pressure.

Video S4: Temporal evolution of void for evolving around an $a_0 = 0.25 \mu\text{m}$ impurity particle with an imposed stripping current $j_\infty = 1 \text{ mA cm}^{-2}$ for a cell subjected to a stack pressure $p = 1 \text{ MPa}$.